



Portable GNSS Software-Defined Receiver Based on ADALM-Pluto SDR

EEE493 Industrial Design Project I Committee Meeting 2 Report

Electrical and Electronics Engineering Department

Group Members: Yiğit Kağan Öztürk, Emre Kurt, Emre Şaş,
Gökay Solak, Awais Ahmad Awan, Berfin Lara Bilgen

Academic Mentor: Asst. Prof. Özlem Tuğfe Demir

Company Mentor: Ahmet Melih Gedikli

Teaching Assistant: Batuhan Uykulu

29.12.2025



VisionX Technology develops AI-powered satellite intelligence systems, including onboard flight computers, smart payload controllers, and edge computing solutions for space missions. The company works across LEO, GEO, and deep-space mission domains, offering expertise in autonomous payload processing, subsystem interface control (SpaceWire, CAN, RS-422/485), and real-time health monitoring and fault resilience.

TABLE OF CONTENTS

ABSTRACT	
LIST OF FIGURES	
LIST OF TABLES	
1. MOTIVATION AND NOVELTY.....	1
2. REQUIREMENTS.....	3
2.1 Functional Requirements:.....	3
2.1.1 Hardware Functional Requirements.....	3
2.1.2 GNSS Signal Algorithms Functional Requirements.....	3
2.1.3 GUI Functional Requirements.....	4
2.2 Non-Functional Requirements/Constraints:.....	4
2.3 The Changes in the Requirements since CM1.....	5
3. OVERALL SYSTEM ARCHITECTURE.....	5
4. METHODS AND IMPLEMENTATION DETAILS.....	5
4.1 Work Packages, Work Breakdown Structure, Project Plan and Milestones.....	5
4.1.1 Work Packages, Work Breakdown Structure and Project Plan.....	5
4.1.1.1 Work Packages.....	5
4.1.1.2 Work Breakdown Structure.....	6
4.1.1.3 Project Timeline.....	6
4.1.2 Milestones and Success Criteria.....	7
4.1.3 Changes Project Plan Since CM1.....	8
4.2 Methods and Progress.....	9
4.2.1 Methods and Tools.....	9
4.2.1.1 Hardware Setup and System Configuration.....	9
4.2.1.1.A Active GNSS Antenna (u-blox ANN-MB2-00).....	9
4.2.1.1.B Bias-Tee (Mini-Circuits ZFBT-4R2G+).....	10
4.2.1.1.C DC Block (Mini-Circuits BLK-89-S+).....	10
4.2.1.1.D External Temperature-Compensated Crystal Oscillator (Epson TG2520SMN) [10].....	11
4.2.1.1.E ADALM-Pluto SDR (AD9363 + Zynq-7010 SoC).....	11
4.2.1.1.F Clock Integration Method.....	12
4.2.1.1.G Hardware focused Risks and Mitigation.....	12
4.2.1.2 Acquisition Method in GNSS Signal Processing.....	13
4.2.1.2.A Signal Reception and Sampling.....	14
4.2.1.2.B Delay–Doppler Search Space Formation.....	14
4.2.1.2.C FFT-Based Acquisition in the Frequency Domain.....	15
4.2.1.2.D Optimization Techniques (Comb, Multi-Frequency).....	16
4.2.1.2.E Detection and Decision.....	17

4.2.1.3 Tracking Method in GNSS Signal Processing.....	17
4.2.1.4 Telemetry Decoding and Data Processing.....	18
4.2.1.5 PVT Computation.....	19
4.2.1.6 GUI Design and System Integration.....	20
4.2.2 Progress and the Current State.....	20
4.2.2.1 Progress up to CM1.....	20
4.2.2.2 Progress up to CM2.....	22
4.2.2.2.1 Synthetic Data Generation.....	22
4.2.2.2.2 Tracking Matlab Simulation.....	23
4.2.2.2.3 GNSS-SDR Monitoring GUI Extension and Preliminary Performance Demonstration.....	23
4.2.2.2.3.1 Extension of the Baseline GNSS-SDR Monitor GUI....	23
4.2.2.2.3.2 Communication Setup and GNSS-SDR Configuration.	24
4.2.2.2.3.3 Implemented GUI Components, Parameter Selection, and Visualization Strategy.....	26
4.2.2.2.3.4 GUI Functionality with Synthetic Dataset Simulation....	27
4.2.3 Future Plans.....	28
4.2.3.1 Validation and Precaution via Gpredict.....	29
4.2.3.2 Planned Horizontal Positioning Error and Uncertainty Analysis....	31
4.2.3.2.1 Reference-Based Horizontal Error Definition (Planned).....	31
4.2.3.2.2 Covariance-Based DRMS Estimation (Planned).....	31
4.2.3.2.3 Planned Calibration and Consistency Assessment.....	33
5. INITIAL PLAN FOR FINAL DEMO.....	33
6. DETAILED EQUIPMENT LIST.....	34
7. REFERENCES.....	35
8. APPENDICES.....	38
Appendix A - Overall System Architecture.....	38
Appendix B - Work Breakdown Structure.....	39
Appendix C - Project Timeline.....	40
Appendix D - Changes on Project Timeline since CM1.....	41
Appendix E - Specifications of Hardware Pack.....	42
Appendix F - Streamed Parameters for PVT Block.....	44
Appendix G - GUI Subsections and Results of Simulation.....	46
Appendix H - Positional Accuracy Metrics.....	52

ABSTRACT

The Portable GNSS Software-Defined Receiver Based on ADALM-Pluto SDR project aims to create a hardware and software integrated GNSS signal processing block that is modular, flexible and low cost. The project aims to achieve acquisition of 6 satellites in 20s and generate position, velocity, and time solutions based on the received satellite signal. In order to achieve it, Adalm-Pluto SDR will be used as an RF receiver front end which receives the L1, K2 band signals and transmits I/Q (In-phase and Quadrature) baseband signal to the host computer for further signal processing. The host PC should run GNU Radio/GNSS SDR to handle signal acquisition, tracking, telemetry decoding and finally PVT solution generation. The aim is to have a horizontal error of at most 20 meters. In terms of development and testing of the system, individual signal processing stages are aimed to be simulated in MATLAB/Simulink and GNU Radio/GNSS SDR environments with prerecorded data. After validation over prerecorded data, it is aimed to be tested on Adalm-Pluto SDR in real life environments. In terms of expected results, it is aimed to ensure that the receiver and individual algorithms satisfy the performance metrics and are organized in a modular/flexible manner.

LIST OF FIGURES

Figure 1: Some global GNSS satellite organizations	1
Figure 2: Overall System Architecture	38
Figure 3: Work Breakdown Structure	39
Figure 4: Project Timeline	40
Figure 5: Changes on Project Timeline since CM1	41
Figure 6: u-blox ANN-MB2-00	9
Figure 7: Simplified ANN-MB2-00 block diagram	10
Figure 8: Mini-Circuits ZFBT-4R2G+ and the circuit inside it	10
Figure 9: Mini-Circuits BLK-89-S+	11
Figure 10: ADALM-Pluto SDR Front-End Device	11
Figure 11: Simplified block diagram of a generic radio frequency front-end	12
Figure 12: Two-Dimensional Search Space of Delay and Doppler Frequency	15
Figure 13: FFT-Based Circular Correlation Block Diagram	16
Figure 14: Generated PCPS Plot and PSD Analysis of Pre-Recorded Data	21
Figure 15: Generated PCPS Plot and PSD Analysis of Pre-Recorded Data	21
Figure 16: Generated PVT Solutions using GNSS SDR.	21
Figure 17: Progress until CM1 (14.11.2025) on Gantt Chart	22
Figure 18: Synthetic data Generation and Simulation Structure	22
Figure 19: Tracking Matlab Simulation: Resulting IQ constellation and C/N ₀ results	23
Figure 20: Extended GNSS-SDR Monitor GUI main window	24
Figure 21: The Monitor block streaming and the PVT block streaming are distinctly indicated in red, while the Telecommand module is highlighted in green (restricted for now)	25
Figure 22: GNSS-SDR configuration file: PVT Block stream settings (left) and Monitor Block Stream Settings (right)	25
Figure 23: GUI preferences panel showing configured port numbers	26
Figure 24: VisionX overview panel displaying receiver status and PVT summary	46
Figure 25: Per-channel monitoring table obtained from the GNSS-SDR Monitor stream	46
Figure 26: I/Q constellation diagrams for selected tracking channels	47
Figure 27: Carrier-to-noise density ratio (C/N ₀) versus time for multiple channels	47

Figure 28: Doppler frequency estimates versus time for multiple channels	48
Figure 29: Map-based visualization of estimated receiver positions	48
Figure 30: Altitude estimates versus time	49
Figure 31: Estimated horizontal position uncertainty (1σ) versus time	49
Figure 32: ENU covariance matrix components versus time	50
Figure 33: ENU velocity components versus time	50
Figure 34: Noisy Synthetic Data GNSS SDR Results. The carrier to noise ratio is reduced now to around 50 dB-Hz.	51
Figure 35: Gpredict Map Interface showing 3 example satellites and their trajectory (yellow dots) and the current added position of EE-Building (Blue Dot)	30
Figure 36: Selected Parameters (Choices Are Given In The Figure 37) Shown In The terminal	30
Figure 37: Parameters Accessible On The Left and Constellation and Parameters Related To Closest Satellite On The Right	30
Figure 38: Illustration of ECEF versus ENU Coordinate Frameworks	32

,

LIST OF TABLES

Table 1: Hardware Functional Requirements	3
Table 2: Algorithm Functional Requirements	3
Table 3: GUI Requirements	4
Table 4: Non-functional Requirements	4
Table 5: Technical Specifications of u-blox ANN-MB2-00	42
Table 6: Technical Specifications of Mini-Circuits ZFBT-4R2G+	42
Table 7: Technical Specifications of ADALM-Pluto SDR and Epson TG2520SMN	43
Table 8: Hardware focused Risks, Impacts and Mitigation solutions	12
Table 9: Acquisition focused Risks, Impacts and Mitigation solutions	17
Table 10: Tracking focused Risks, Impacts and Mitigation solutions	18
Table 11: Telemetry decoding focused Risks, Impacts and Mitigation solutions	18
Table 12: PVT algorithm focused Risks, Impacts and Mitigation solutions	19
Table 13: GUI focused Risks, Impacts and Mitigation solutions	20
Table 14: Complete list of streamed parameters from PVT Block	44
Table 15: Results obtained on GUI through Synthetic Dataset Simulation	27
Table 16: Available Positional Accuracy metrics for GNSS signals	52
Table 17: Calibration Ratios and their Implications	33
Table 18: Detailed equipment list and costs	34

1. MOTIVATION AND NOVELTY

The Portable GNSS Software-Defined Receiver Based on ADALM-Pluto SDR project mainly focuses on developing a low cost, hardware and software integrated, modular GNSS signal processing block that can be updated and modulated based on possible future applications.

The core expectations on the project can be listed as the software and hardware infrastructure being flexible, fully open source and with a considerably low cost. Since the available stand-alone GNSS signal processing products on the market are not promising, these three expectations simultaneously are what the project aims to provide in a GNSS signal processing system that can perform signal processing required for GNSS applications in a modular manner and with a considerably lower cost.

The project comes out as being crucial in terms of contributing to the national expertise on space missions and technologies. The main operating satellite systems in the global scale can be exemplified as GALILEO which is operated and funded by European Union, GPS which is operated and funded by USA, GLONASS established by USSR and operated and funded by Russia, BEIDOU operated and funded by China, QZSS operated and funded by Japan and many more [1].



Figure 1: Some global GNSS satellite organizations [1].

Regarding the GNSS space applications, the main providers can be observed as global actors, countries, and organizations. Therefore, from a national perspective contributing to national space expertise can be regarded as a crucial aspect of Portable GNSS Software-Defined Receiver Based on ADALM-Pluto SDR project.

Moreover, from the market's, developers' and GNSS enthusiasts' perspective, the project aims to provide the community with an operational GNSS signal processing hardware and software block that has portability, modularity, flexibility features with a considerably low cost aiming to enhance the development of efficient and accessible GNSS signal processing systems.

This project not only serves VisionX, but also engineers, researchers and academic groups working with GNSS signals. Since these users are expected to have the basic knowledge related to GNSS applications and the SDR receivers, giving them a configurable and relatively cheap solution is important. Unlike most of the commercial receivers, our project is not a black box. One can access all the processes and parameters freely. Therefore, our project is an open-source alternative

to commercial and research-based GNSS receivers and high-end SDR platforms typically priced above 1000 USD.

The commercial and research-based GNSS receivers and signal processing blocks. To exemplify some commercial products, manufacturers such as Qualcomm, u-blox, and Septentrio provide GNSS receiver and signal processing modules. Closed source (with embedded firmware), algorithms and data access are limited. They deliver high accuracy but are restricted in terms of customizability and cost. To exemplify, mosaic-go X5 GNSS module receiver evaluation kit including only the signal processing block costing 1300 USD comparing with the expected cost of Portable GNSS Software-Defined Receiver Based on ADALM-Pluto SDR as 450 USD with all hardware and software packs, comes out as considerably expensive and having limited modularity and accessibility [2]. Additionally, research-oriented products on the market such as USRP Ettus, bladeRF, and HackRF are widely used in GNSS research. Although they are highly flexible, they are considerably expensive, for example USRP B210 costs 1700 USD [3]. Hence, the novelty of the Portable GNSS Software-Defined Receiver Based on ADALM-Pluto SDR project comes out as promising modularity, flexibility and efficiency with a considerably low cost simultaneously.

A preliminary patent search shows that some sub parts of the Portable GNSS Software Defined Receiver Based on ADALM-Pluto SDR are already patented by different solutions. Therefore, receiving a patent on the project alone is unlikely. To exemplify, there are patented real-time GNSS software receivers [4], [5] and low-power, low-cost GNSS receiver architectures [6]. Additionally, some open-source GNSS-SDR frameworks already support ADALM-Pluto as a front end, indicating that the combination of Pluto SDR and GNSS signal processing may not be regarded as enough for receiving a patent. However, possible addition of custom signal processing accelerators such as Kalman Filter or machine learning based blocks may improve the likelihood to get a patent. These accelerators are in consideration.

SDR based receiver structures support high modularity and flexibility, where in space missions the modularity and software-based improvement instead of direct hardware-based interference is more preferable. Hence, software defined GNSS receivers are promising in terms of space missions, on board satellite computers and even ground receiver terminals. Regarding these aspects VisionX Technology, whose main occupation is in development of satellite on board flight computers, comes out as being eager to integrate SDR based GNSS products into their systems. Hence, Portable GNSS Software-Defined Receiver Based on ADALM-Pluto SDR project's developed software and hardware infrastructure with probable research and development phase is aimed to be integrated with preexisting systems and expected to be integrated in ongoing developments for the satellite on board computer for Gezgin 1 which is planned to be launched in 2028. Additionally, the developed software and hardware infrastructure and know-how is aimed to be used for real-time positioning and time synchronization for CubeSat and microsatellite platforms in future. Consequently, VisionX Technology aims to gain infrastructure and know-how on the SDR based GNSS signal processing blocks at the end of the project to develop SDR based subsystems for space missions.

2. REQUIREMENTS

The purpose of this system is to develop a software-defined GNSS receiver capable of acquiring, tracking, and computing position velocity and time (PVT) solutions from L1 and L2 band GNSS signals using a single SDR device for RF front end. The SDR device serves as an RF front-end connected to a host PC running Ubuntu 22.04. The system will operate with the open-source GNU Radio and GNSS-SDR frameworks. The host PC runs GNU Radio and GNSS-SDR, which perform acquisition, tracking, and PVT calculation.

The system should be able to:

- I. Receive and digitize and transmit GNSS frequency bands (GPS L1 and GPS L2).
- II. Acquire and track signals from at least six visible satellites.
- III. Compute position solutions within 20s (cold start).
- IV. Achieve $\leq 20\text{m}$ radial position accuracy in open-sky conditions.

2.1 Functional Requirements:

2.1.1 Hardware Functional Requirements

Table 1: Hardware Functional Requirements

ID	Requirement	Requirement Statement
HW-FR-1	Data Transmission Requirement.	Data transmission rate $> 4 \text{ MSPS}$.
HW-FR-2	Local Oscillator Stability Requirement.	The internal LO should maintain frequency stability within $\pm 1 \text{ ppm}$ over $0\text{--}40^\circ\text{C}$.
HW-FR-3	Bandwidth Requirement	The hardware must receive 1575.42 MHz and 1227.6 MHz signals and down convert it to 2 MHz baseband signal.

2.1.2 GNSS Signal Algorithms Functional Requirements

Table 2: Algorithm Functional Requirements

ID	Requirement	Requirement Statement
ACQFR-1	Signal Detection	The acquisition module shall detect and identify signals from at least six GNSS satellites within 20 seconds after startup.
TRKFR-1	Lock Maintenance	Tracking module maintains a carrier and code lock for at least 6 satellites.
PVTFR-1	Position Accuracy	Navigation module shall compute 3D position and velocity once per second with $\leq 20\text{m}$ RMS horizontal error under open-sky conditions.

PVTFR-2	Data Logging	The system shall store PVT solutions, acquired satellites, and tracking data with synchronized timestamps.
---------	--------------	--

2.1.3 GUI Functional Requirements

Table 3: GUI Requirements

ID	Requirement	Requirement Statement
GUI-R-1	CNR Display	The GUI shall display the estimated C/N ₀ (CNR).
GUI-R-2	Satellite Constellation View	The user interface shall display real-time satellite constellation tracking within 1s of update.
GUI-R-3	Satellite Count Indicator	The GUI shall exhibit the acquired number of satellites.
GUI-R-4	Position Display	The GUI will show the computed position updated every 1s.

2.2 Non-Functional Requirements/Constraints:

Table 4: Non-functional Requirements

ID	Requirement	Requirement Statement
NFR-1	Maximum allowable cost	Less than 1000 USD.
NFR-2	Maximum allowable size, weight	Not Applicable
NFR-3	Power requirement/constraint	Not Applicable
NFR-4	Environmental operating conditions and other issues	The receiver shall operate under -10 °C to +50 °C, 0–85 % RH, and resist mild vibration and sunlight exposure during outdoor field tests.
NFR-5	Safety issues	The design shall ensure electrical and RF safety, including proper grounding, ESD protection, and safe antenna voltage biasing (< 5 V).
NFR-6	Health constraints and requirements	Not applicable.
NFR-7	Global, cultural, and social factors	Global applicability and open-source collaboration
NFR-8	References related to the standards that the product will be compatible with	EMC Directive 2014/30/EU, RoHS 2 Directive 2011/65/EU, IEC 60950-1:2005

2.3 The Changes in the Requirements since CM1

As can be seen in Table 1, HW-FR-3 is added to the hardware requirements. This requirement denotes the operating frequency of the receiver.

In addition, the software requirements (coded with SW-FR-1 and SW-FR-2) are removed. Those requirements indicated the design choice of the project, they were not requirements.

3. OVERALL SYSTEM ARCHITECTURE

In this section, the project's overall software and hardware architecture of the project is explained. For schematic of the overall architecture regard Appendix A Figure 2. The architecture covers both software and hardware chain involving active antenna, antenna DC supply, intermediate bias tee and dc block connections with the Adalm Pluto SDR powered by host PC USB 2.0 power line. The power, RF signal, control and data stream connections and formats are indicated. Regarding the software infrastructure basic GNSS SDR signal processing flow which will be running in the Linux OS PC exhibited. The essential signal conditioner blocks, acquisition and tracking channels, telemetry decoding, observable generation and PVT solution blocks clearly shown. Additionally, the custom GUI added to the overall structure.

4. METHODS AND IMPLEMENTATION DETAILS

In this section, the project's main work packages and plans are explained. In the subsequent subsection, the methods, tools and progress on the project are explained.

4.1 Work Packages, Work Breakdown Structure, Project Plan and Milestones

In this subsection the work packages, work breakdown structure, project plan are explained. The milestones and related success criteria are explained. The relation between work packages and milestones are given and the related success criteria are examined.

4.1.1 Work Packages, Work Breakdown Structure and Project Plan

4.1.1.1 Work Packages

The project is organized into six main work packages, each representing a core functional block of the GNSS software-defined receiver. These work packages allow parallel development of hardware, signal-processing algorithms, and software modules while ensuring that all components can later be integrated into a unified system.

WP1 – Hardware Setup and System Configuration: This work package includes the selection and integration of all RF front-end components such as the active GNSS antenna, bias-tee, DC block, and ADALM-Pluto SDR. It also covers the external TCXO clock integration, SDR parameter configuration (frequency, gain, sampling rate), and initial I/Q data capture tests. WP1 establishes the physical and digital foundation required for all subsequent work packages.

WP2 – Acquisition Module Development: WP2 focuses on the design and implementation of GNSS satellite acquisition algorithms using GNSS-SDR. Tasks include delay-Doppler search implementation, FFT-based correlation, thresholding logic, and verification of acquisition time and C/N₀ performance using prerecorded datasets. This work package ensures the system can correctly identify visible satellites and provide initial signal parameters.

WP3 – Tracking Module Development: This work package involves implementing DLL, FLL, and PLL tracking loops to maintain continuous synchronization with acquired satellites. Activities include loop filter configuration, carrier/code tracking validation, stability checks under varying signal conditions, and real-time tuning for optimal lock performance.

WP4 – Telemetry Decoding and Data Processing: WP4 covers the extraction of navigation message bits from the tracked signals. Tasks include frame synchronization, parity checking, ephemeris decoding, and preparing cleaned navigation data for the PVT module. This package ensures accurate observables and timing data are available for position computation.

WP5 – PVT Computation: This work package focuses on computing the receiver's position, velocity, and time using decoded satellite data. Tasks include pseudorange calculation, least-squares position estimation, clock bias correction, and verification of horizontal error performance against expected metrics.

WP6 – GUI Design and System Integration: WP6 includes the development of a lightweight Python-based GUI to visualize system outputs such as C/N₀, satellite count, constellation view, and 1 Hz position updates. It also covers the integration of all work packages into a seamless end-to-end receiver pipeline. This is the final phase and will be completed after acquisition, tracking, and PVT modules are fully validated.

4.1.1.2 Work Breakdown Structure

The work breakdown structure of the project is constructed aligned with the work packages. The main categories of the structure of the project are work packages. Each work package is divided into subcategories to track the timeline of the project and equally distribute the work among the group members. These subcategories are named in each work package. The work breakdown structure can be found in Appendix B Figure 3.

4.1.1.3 Project Timeline

The project timeline is the time-stamped version of the work breakdown structure. The Gantt-style timeline shows the planned start and end weeks across the academic year, covering Fall, the semester break, and Spring. This visual layout helps track progress, coordinate parallel work, and align module-level development with milestone deadlines such as CM1, L1–L3, and CM2. It can be found in Appendix C, Figure 4.

4.1.2 Milestones and Success Criteria

Work packages and milestones of the project are aligned and they are the same. For the milestones (work packages), some crucial tasks are determined and success criteria for each milestone are defined.

WP1 – Hardware Setup and System Configuration

Main tasks for WP1 are:

- ADALM-Pluto SDR integration with active antenna, bias-tee, and DC block.
- External 40 MHz TCXO reference connection and I/Q streaming verification

The success criteria for this work package are:

- Real-time I/Q streaming rate > 4 MSPS without packet loss (HW-FR-1).
- Local oscillator stability within ± 1 ppm over 0–40 °C (HW-FR-2).
- RX channel digitizes GNSS L1/L2 signals (HW-FR-3).

WP2 – Acquisition Module Development

Main tasks for WP2 are:

- Implementation of correlation-based search for satellite detection.
- Validation of acquisition time and C/N₀ performance.

The success criteria for this work package are:

- At least six GNSS satellites detected within 20 s of startup (ACQFR-1).
- Average C/N₀ > 40 dB-Hz under open-sky conditions [14].
- SDR configuration and frequency control performed by software.

WP3 – Tracking Module Development

Main tasks for WP3 are:

- PLL/DLL loop design and implementation for carrier/code tracking.
- Tracking stability evaluation under real-time operation.

The success criteria for this work package are:

- Continuous lock maintained for ≥ 60 s when C/N₀ > 25 dB-Hz (TRKFR-1).
- Tracking loops remain phase-stable within ± 0.5 Hz frequency drift.

WP4 – Telemetry Decoding and Data Processing

Main tasks for WP4 are:

- Navigation message bit extraction and time decoding.
- Validation with real GNSS datasets.

The success criteria for this work package are:

- Navigation data correctly decoded and ephemeris validated.

- Modular GNSS-SDR architecture maintained across acquisition, tracking, and navigation blocks.

WP5 – PVT Computation

Main tasks for WP5 are:

- Pseudorange and geometry computation.
- Position, velocity, and time estimation.

The success criteria for this work package are:

- 3D position and velocity computed once per second with ≤ 20 m RMS error (PVTFR-1).
- PVT data logged with synchronized timestamps (PVTFR-2).

WP6 – GUI Design and System Integration

Main tasks for WP6 are:

- GUI layout and visualization of satellites, C/N₀, and computed position
- Integration of acquisition, tracking, and PVT outputs

The success criteria for this work package are:

- GUI displays real-time C/N₀ levels (GUI-R-1).
- Constellation view updated within 1 second (GUI-R-2).
- Satellite count indicator and position updated every 1 second (GUI-R-3, GUI-R-4).

4.1.3 Changes Project Plan Since CM1

In the project timeline, there are five main changes:

- The first one is changing the data for simulation of the algorithms. Recorded data is not available in the online sources. They are either encrypted by the author or encrypted by the recording device which can be only decoded with the similar product's service. Therefore, synthetic data is generated and used to test the algorithms.
- The starting and the ending date of the hardware related parts are postponed (WP 1) since the hardware components haven't reached us.
- The ending date of the validation of acquisition time and SNR performance (task of WP2) is extended.
- The starting date of the telemetry decoding and data processing (WP4) is postponed.
- The starting date of GUI design phase, and integration of GUI with PVT and monitoring modules is shifted to early phases of the project (WP6).

One can see the changes in Appendix D Figure 5.

4.2 Methods and Progress

In this section, the methods and tools relevant to the project's work packages and the group's progress will be discussed.

4.2.1 Methods and Tools

4.2.1.1 Hardware Setup and System Configuration

The hardware infrastructure of the Portable GNSS Software-Defined Receiver is designed to create a stable, low-noise, and modular RF front-end capable of reliably receiving GPS L1 and L2 signals (HW-FR-3) and streaming digitized I/Q samples to the host PC for processing. The chosen hardware elements including active GNSS antenna, bias-tee, DC block, ADALM-Pluto SDR, and an external TCXO, together form a coherent reception chain that meets the functional requirements HW-FR-1 (4 MSPS streaming) and HW-FR-2 (± 1 ppm LO stability). In this context, the datasheets of the possible equipment set were studied and working principles were understood and explained.

Strategy: The strategy that will be used for WP1 can be explained as building a stable hardware chain first, then validating with short I/Q captures and checks (spectrum, quantization, gain behavior).

4.2.1.1.A Active GNSS Antenna (u-blox ANN-MB2-00) [7]



Figure 6: u-blox ANN-MB2-00

The ANN-MB2-00 is the primary RF sensor of the system. GNSS signals arriving at Earth have extremely low power levels (typically -130 to -140 dBm). To make these signals detectable by the SDR, the antenna integrates the following internal functions which are also summarized in Figure 7:

- i. **Ceramic Patch Radiator (RHCP):** It is designed for Right-Hand Circular Polarization to match satellite transmission, improve sky visibility, and reduce multipath from the ground.
- ii. **SAW Band-Pass Filters (L1/L2/L5 Bands):** Narrowband filters suppress out-of-band interference (LTE, Wi-Fi, ISM bands), reducing the effective noise bandwidth.
- iii. **Low-Noise Amplifier (LNA):** The LNA provides ~ 30 dB gain with 2.5–3 dB noise figure, boosting the weak GNSS signals before cable losses (~ 5 –6 dB) and thus dominates the receiver noise figure. By amplifying first, the LNA

effectively “raises” the signal above the noise introduced later by the cable and SDR input.

- iv. **Integrated Bias Network:** It accepts 3–5 V DC through the coaxial cable to power the LNA.

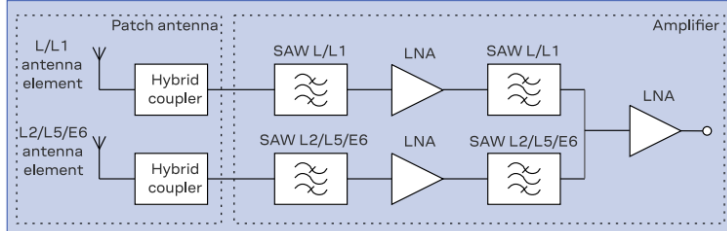


Figure 7: Simplified ANN-MB2-00 block diagram

The summary for technical specifications of the u-blox ANN-MB2-00 can be found in Appendix E, Table 5.

4.2.1.1.B Bias-Tee (Mini-Circuits ZFBT-4R2G+) [8]

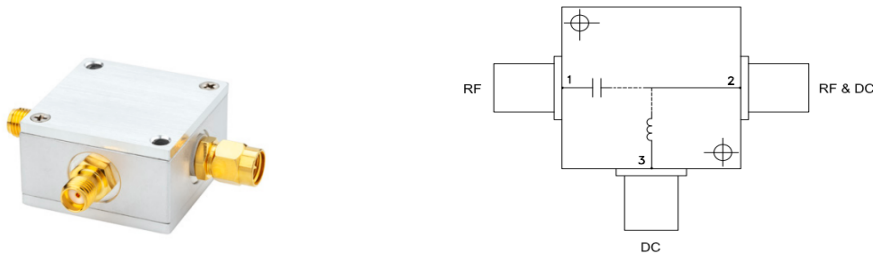


Figure 8: Mini-Circuits ZFBT-4R2G+ and the circuit inside it.

Since the ADALM-Pluto does not provide bias voltage to power the antenna LNA, a bias-tee is inserted between the antenna and the SDR. The internal working principle is given in Figure 8. The Inductor Arm allows DC while blocking RF signal whereas Capacitor Arm passes RF while blocking DC. This ensures the antenna receives power but the SDR input remains fully DC-isolated. Summary of technical specifications for Bias-T can be found in Appendix E, Table 6.

4.2.1.1.C DC Block (Mini-Circuits BLK-89-S+) [9]

In our GNSS receiver chain, a DC block is inserted between the bias-tee and the Pluto SDR to protect the RF input stage against potential DC leakage or voltage spikes. The DC block uses a high-quality series capacitor to provide complete DC isolation while maintaining RF transparency from 0.1–8000 MHz and introducing negligible insertion loss (<0.1 dB).



Figure 9: Mini-Circuits BLK-89-S+

This prevents accidental damage from bias-tee power or wiring mistakes and ensures long-term safety during outdoor testing (aligned with NFR-5).

4.2.1.1.D External Temperature-Compensated Crystal Oscillator (Epson TG2520SMN) [10]

(Explained in the subsequent section)

4.2.1.1.E ADALM-Pluto SDR (AD9363 + Zynq-7010 SoC) [2]

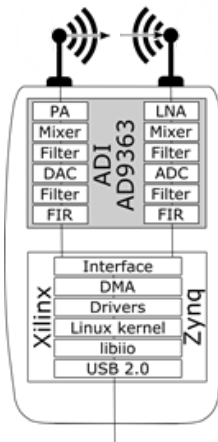


Figure 10: ADALM-Pluto SDR Front-End Device

The ADALM-Pluto SDR functions as the primary RF front-end and digitization platform of the GNSS receiver. Based on the AD9363 RF Agile Transceiver and Zynq-7010 SoC, Pluto performs RF tuning, analog filtering, automatic gain control, quadrature mixing, and 12-bit I/Q digitization required for GNSS L1/L2 processing. After downconversion, the Pluto streams continuous baseband I/Q samples to the host PC through USB 2.0, where main algorithm blocks are executed using GNU Radio and GNSS-SDR. Full software control over the SDR, including center frequency, sampling rate, RF gain, and digital filter bandwidth, supports the modular structure and ensures that the hardware front-end is fully configurable for different GNSS signals and test conditions. Figure 11 illustrates this workflow in a block diagram.

One thing to note is that for GNSS applications, frequency stability is a critical factor. Pluto's default 40 MHz crystal exhibits ± 25 ppm stability, leading to local

oscillator drift, carrier tracking instability, and degraded Doppler accuracy, especially noticeable in weak-signal environments. To ensure compliance with HW-FR-2 (LO stability $\leq \pm 1$ ppm), the SDR is upgraded with an external Epson TG2520SMN 40 MHz Temperature-Compensated Crystal Oscillator (TCXO). The TG2520SMN provides ± 0.5 ppm stability over a wide thermal range, as well as significantly lower phase noise. This improves PLL/DLL stability, extending coherent integration times, and enabling consistent multi-satellite tracking under real operating conditions.

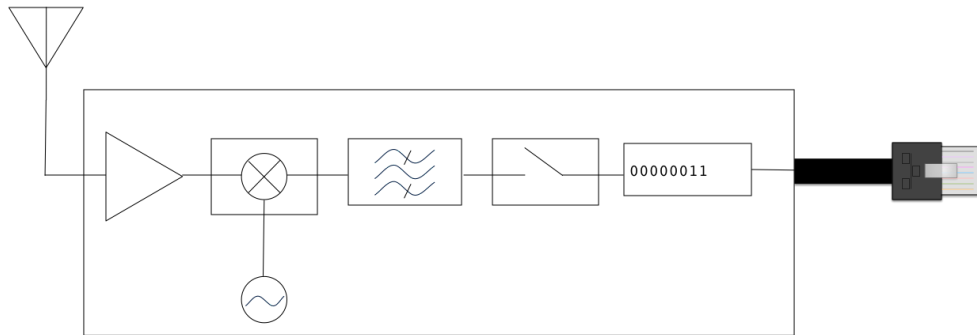


Figure 11: Simplified block diagram of a generic radio frequency front-end.

Summary of technical specifications for both ADALM-Pluto SDR and External TCXO can be found in Appendix E, Table 7.

4.2.1.1.F Clock Integration Method

The integration of the external TCXO into the Pluto SDR is performed using the supported reference-clock override path of the AD9363 transceiver. In this project, the external TG2520SMN TCXO is connected to the SDR through its reference-clock port, allowing Pluto to operate entirely based on the TCXO's stable frequency source.

This integration approach does not require destructive hardware modification and as a result, the SDR benefits from a high-stability, low-phase-noise master clock, improving Doppler estimation, reducing carrier phase jitter, and ensuring the timing accuracy needed for reliable GNSS acquisition and tracking.

4.2.1.1.G Hardware focused Risks and Mitigation

Table 8, summarizes the risks associated with the initial Hardware setup and testing phase, their corresponding impacts and possible mitigation solutions:

Table 8: Hardware focused Risks, Impacts and Mitigation solutions

Risk	Impact	Mitigation
LO drift or thermal instability	Loss of carrier/code lock	TCXO upgrade, periodic calibration
Low C/N ₀ due to cable loss or multipath	Acquisition failure	Short coax, outdoor placement, ground-plane mounting

DC leakage into SDR	Permanent hardware damage	DC block and bias-tee isolation
USB throughput bottleneck	Packet loss > 4 MSPS	Project requirement restricted to GPS L1/L2 bands
Antenna power failure	No reception	Current monitoring at bias-tee DC port
Interference in urban field	False acquisition peaks	SAW filtering and controlled test locations

In addition, since there is a possibility of failure that can break the whole RF pipeline or ADALM-Pluto itself, all the hardware parts have their backup. For the clock, more than enough backup was made and one variant of TCXO is added which may be used for testing.

Software and techniques: Pluto SDR tools (IIO/Soapy/SDR software), GNSS-SDR signal source config, test captures at correct center frequency and sample rate, verify I/Q format and clipping (gain setting).

Outputs to be Verified: Confirm clean L1/E1 reception, correct sampling, stable clock lock, repeatable I/Q recordings usable by WP2–WP5.

Accomplishment until now: The review and set up plan for all hardware components are done and waiting for the pack to be delivered.

4.2.1.2 Acquisition Method in GNSS Signal Processing

The acquisition process is the first functional stage of a Global Navigation Satellite System (GNSS) receiver. Its main purpose is to detect which satellites are currently visible and to determine their approximate code phase and Doppler frequency. These parameters are required to synchronize the locally generated replica signal with the incoming satellite transmission. Acquisition operates as a search procedure over possible time delays and frequency offsets that result from satellite motion, receiver dynamics, and clock differences. Successful acquisition ensures that the receiver can proceed to the tracking stage, where finer synchronization and continuous signal monitoring occur.

Because acquisition directly affects both sensitivity and Time to First Fix (TTFF), many algorithms have been proposed to optimize its performance. The classical method is based on direct correlation, where the received signal is compared with locally generated pseudorandom (PRN) codes for each satellite. However, this method is computationally demanding, so more efficient techniques such as Fast Fourier Transform (FFT)-based correlation have been developed to evaluate all code delays in parallel. Advanced implementations further reduce complexity by using methods such as circular correlation, serial and parallel code-phase search, and optimization filters like Comb or Cascaded Integrator–Comb (CIC) filters. In addition, modern multi-frequency and multi-constellation receivers perform acquisition across several signal bands simultaneously to improve robustness and speed.

Therefore, the acquisition process in GNSS can be viewed as a sequential chain of operations: first defining the delay–Doppler search space, then applying correlation through either time-domain or frequency-domain methods, and finally optimizing detection by thresholding and resource-efficient filtering. The following sections describe each of these methodological steps in detail, outlining how they collectively form the foundation of signal detection in contemporary GNSS receivers.

4.2.1.2.A Signal Reception and Sampling

The acquisition process begins with receiving and digitizing the weak GNSS signals transmitted by multiple satellites. These signals contain a carrier, a pseudorandom (PRN) code, and navigation data, and they arrive at Earth with very low power, around -160 dBW. The receiver first amplifies and down-converts them to a manageable intermediate frequency (IF) using a low-noise front end [15].

After filtering out unwanted noise, the analog signal is sampled by an analog-to-digital converter (ADC) to create a stream of digital data, often represented in I/Q format. These samples contain the complete satellite information, but with unknown code delay and Doppler frequency values. [15]

This stage provides the digital input required for acquisition algorithms. The next section focuses on forming the delay–Doppler search space, where the receiver tests various time and frequency hypotheses to identify and align with the incoming satellite signals.

4.2.1.2.B Delay–Doppler Search Space Formation

Once the GNSS signal is digitized, the receiver must identify two unknown parameters that define its alignment: the code delay and the Doppler frequency shift. These parameters determine how much the incoming signal is delayed in time and shifted in frequency compared to the locally generated replica. To estimate them, the receiver constructs a delay–Doppler search space, a two-dimensional grid containing all possible combinations of code delay and Doppler hypotheses .

Each cell in this grid represents one hypothesis pair. The receiver evaluates the correlation between the incoming signal and a locally generated replica for each cell. A strong correlation peak indicates the correct alignment, meaning the signal from a specific satellite has been successfully detected. The horizontal axis of the grid corresponds to possible code delays (τ), and the vertical axis represents Doppler frequencies (f_D). The resolution of this grid depends on the integration time, sampling frequency, and the expected Doppler range. Smaller bin sizes increase accuracy but also raise computational cost .

Figure 12 illustrates the delay–Doppler plane explored during acquisition. Each square (bin) represents one unique combination of code delay and Doppler frequency. The central darker cell marks the correct correlation peak where the receiver's local code and carrier align with the incoming signal.

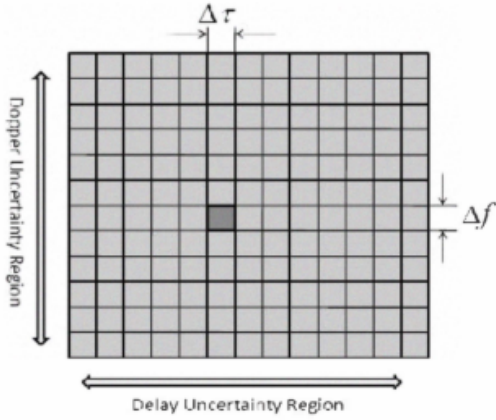


Figure 12: Two-Dimensional Search Space of Delay and Doppler Frequency [15]

This method provides an intuitive time-domain interpretation of acquisition: the receiver “slides” the local replica step by step, both in frequency and code phase. Because of its computational complexity, this algorithm is not used in the project. Although the algorithm used in the project for acquisition is parallel code phase search (PCPS), knowing the basics of this algorithm is useful for interpretation of PCPS.

4.2.1.2.C FFT-Based Acquisition in the Frequency Domain

The computational complexity of circular and serial correlation in the time domain makes them inefficient for real-time GNSS signal processing. To overcome this limitation, modern receivers employ the Fast Fourier Transform (FFT), which allows the correlation to be calculated in the frequency domain instead of the time domain. The convolution theorem provides the theoretical basis for this approach, stating that correlation in the time domain is equivalent to multiplication in the frequency domain. This means that by transforming both the received signal and the locally generated code into the frequency domain, correlation can be achieved more efficiently through spectral multiplication followed by an inverse FFT [16].

In the FFT-based approach, the incoming digitized intermediate-frequency (IF) signal $y_{IF}(n)$ and the locally generated code $y_c(n)$ are first transformed using FFT:

$$Z(k) = Y_c(k) \cdot Y(k)_{IF}^*$$

where $Y_{IF}^*(k)$ and $Y_c(k)$ denote the FFTs of the received and local signals. Since taking conjugate in frequency domain means time reversal in the time domain circular correlation is equal to multiplying Y_c and conjugate of Y_{IF} .

The time-domain correlation result is then recovered using the inverse FFT (IFFT):

$$z(n) = \text{IFFT}\{Z(k)\}$$

The peak of $|z(n)|$ identifies the correct code delay and Doppler frequency, completing the acquisition process [16].

FFT-based acquisition reduces computational complexity from the order of N^2 in the serial search to the Order of $N \log \log N$ in the frequency domain. This allows real-time acquisition even for long PRN sequences and multiple satellites. In addition, FFT-based approaches reuse the same processing modules for both FFT and IFFT. FFT-based model gets rid of the calculation burden of τ , but it cannot get rid of the Doppler frequency calculation.

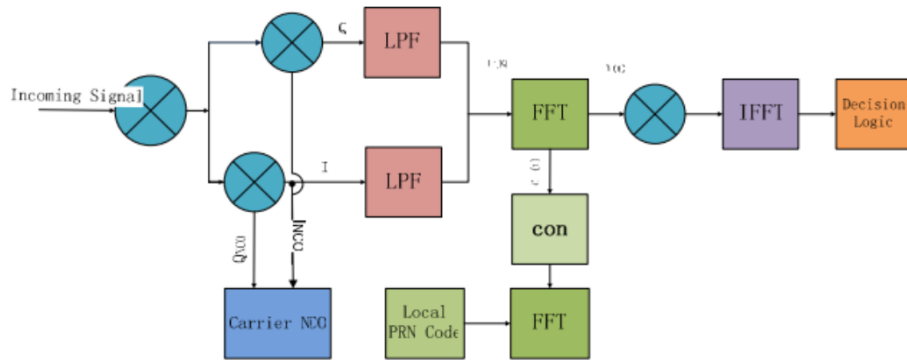


Figure 13: FFT-Based Circular Correlation Block Diagram [16]

To acquire multiple satellites or frequency bands, modern receivers perform FFT-based correlation across several Doppler bins in parallel. Each Doppler bin corresponds to a frequency offset hypothesis that is removed by pre-mixing the IF signal before FFT processing. The resulting two-dimensional correlation surface provides the maximum likelihood estimate of both delay and frequency.

4.2.1.2.D Optimization Techniques (Comb, Multi-Frequency)

The process of simultaneously utilizing GNSS signals provided on various frequency bands, such as GPS L1 C/A, L2C, and L5, to increase the acquisition stage's speed, sensitivity, and resilience is known as multi-frequency acquisition. Each satellite in a modern GNSS constellation (such as GPS, Galileo, and BeiDou) broadcasts numerous signals, each of which is scaled according to carrier frequency but experiences the same underlying satellite-to-receiver dynamics, particularly Doppler shift and code delay. By utilizing these common characteristics, multi-frequency acquisition greatly narrows the search space and enhances detection efficiency [17]. Since the Doppler shift is proportional to the signal's carrier frequency, once Doppler is estimated on one frequency, the Doppler search window on other frequencies can be reduced to a very narrow interval. This reduces the computational load [17]. Multi-frequency approaches can combine signals in two

ways, which are noncoherent and coherent combining [17]. Phase-aligned signals from different frequencies are combined before correlation.

4.2.1.2.E Detection and Decision

The receiver must determine whether a correlation peak represents a real satellite signal or only noise after the acquisition stage calculates the correlation values over all code phases and Doppler bins. A binary hypothesis test is used to formulate this decision-making process. The null hypothesis is there is noise only (no satellite present), and the alternative hypothesis is there is signal plus noise (satellite present). For each Doppler bin, the maximum correlation value is extracted, and the global peak P is selected. Then the corresponding (τ, f_D) represent the estimated code delay and Doppler [18]. For many receivers, it is common to normalize the metrics. It should be checked whether it meets the threshold criteria. The threshold is chosen to satisfy the false alarm probability [19]. If the detection criteria is satisfied, the receiver states that the satellite acquired and transmits the estimated code delay and Doppler to the tracking loops (DLL/PLL/FLL). If not, the search proceeds and the PRN is marked as absent.

This phase directly affects sensitivity and time-to-first-fix (TTFF) by guaranteeing accurate satellite detection and preventing spurious acquisitions [20]. In addition to the previous discussion, Table 9, details the acquisition focused risks and the respective mitigation strategies.

Table 9: Acquisition focused Risks, Impacts and Mitigation solutions

Risk	Impact	Mitigation
False acquisition due to noise or multipath interference.	Faulty, misleading acquisition may slow the navigation chain.	Apply adaptive detection threshold, cross-correlation validation.

Strategy: The key strategy that will be employed for hardware integration corresponding to WP1 can be explained as implementing and validating acquisition: stable and reliable delay and doppler grid search through FFT-based correlation PCPS algorithm, decision rule based on threshold decision and reporting PRN, Doppler, code phase.

Tools and software: GNSS-SDR acquisition blocks will be used and fine tuned with synthetic datasets before getting hardware packs.

Simulations and verification: To verify WP2 acquisition algorithm will be run on synthetic clean and noisy data and acquisition time and detection reliability will be measured.

Key outputs: Correct satellite detection list with reasonable doppler and code phase and acceptable acquisition time and C/N₀ behavior will be targeted.

Accomplishment until now: Acquisition module tested over synthetic clear and noisy data and it exhibited reasonable success, Moreover, fine tuning and modifications on the module planned to increase time efficiency.

4.2.1.3 Tracking Method in GNSS Signal Processing

The tracking process ensures accurate Doppler frequency shift and the code phase shift due to relative velocities of the receiver and the satellite. The tracking process is planned to be achieved by using DLL (delay locked loop) for PRN code phase lock, and a FLL (frequency locked loop) for the carrier frequency lock regarding GPS L1 and L2 signal structure. Table 10 details the tracking focused risks and the respective mitigation strategies.

Table 10: Tracking focused Risks, Impacts and Mitigation solutions

Risk	Impact	Mitigation
Loss of lock under low CNR conditions.	Telemetry decoding fails.	Efficient signal conditioning, digital filtering can be used to improve performance.

Strategy: The strategy for tracking module development corresponding to WP3 is to maintain continuous synchronization with acquired satellites by configuring and tuning code and carrier tracking loops. DLL, FLL, and PLL structures are adjusted to ensure stable lock under varying signal conditions.

Tools and software: GNSS-SDR tracking blocks with configurable loop filters and discriminators are used. Tracking diagnostics such as lock indicators and loop error outputs are monitored.

Simulations and verification: Tracking performance is evaluated using prerecorded datasets with different signal strengths. Loop stability, loss-of-lock events, and C/N₀ evolution are analyzed.

Key outputs: Stable carrier and code tracking with continuous lock, producing accurate observables for telemetry decoding.

Accomplishment until now: Tracking module block successfully configured for gnss sdr and validated with synthetic clear and noisy data. It is planned to be fine tuned to achieve higher timing efficiency.

4.2.1.4 Telemetry Decoding and Data Processing

When the tracking loop ensures the lock on the satellite signal, the base-band signal is decoded for acquiring the navigation data from the satellite. This process involves frame synchronization, parity checking, and data extraction for observable, clock corrections, and gathering almanac information. Table 11 details the telemetry focused risks and the respective mitigation strategies.

Table 11: Telemetry decoding focused Risks, Impacts and Mitigation solutions

Risk	Impact	Mitigation
------	--------	------------

Bit error due to clock jitters or loss of synchronization.	Loss of observable data.	Error checking (parity check, soft decision decoding) can be regarded.
--	--------------------------	--

Strategy and method: The strategy for telemetry decoding corresponding to WP4 is to extract navigation data from the tracked GNSS signals using standard frame synchronization and error-checking procedures. Decoded messages are validated before being forwarded to the PVT stage.

Tools and software: GNSS-SDR telemetry decoder blocks are used for frame synchronization, parity checking, and ephemeris decoding.

Techniques and Verification: Validate frame synchronization rate, parity/pass statistics, ephemeris field plausibility (e.g., week number, toe/toe ranges).

Key outputs: Correctly decoded navigation data, including ephemeris and timing information, ready for PVT computation.

Accomplishment until now: GPS L1 telemetry decoding block configured and integrated to GNSS SDR and validated on clear and noisy synthetic data.

4.2.1.5 PVT Computation

The PVT solver stage of GNSS signal processing generates estimates for position, velocity, and time solutions, given at least four satellites' observables from navigation data. Table 12 details the PVT computation focused risks and the respective mitigation strategies.

Table 12: PVT algorithm focused Risks, Impacts and Mitigation solutions

Risk	Impact	Mitigation
Numerical instability or inconsistent observables	Faulty PVT solutions outputted in the GUI.	Use hybrid observables and perform cross-checking for outliers

Strategy and method: The strategy for PVT computation corresponding to WP5 is to compute the receiver's position, velocity, and time using tracking observables and decoded satellite data. A least-squares estimation method is applied with clock bias correction.

Tools and software: GNSS-SDR PVT outputs and MATLAB/Python scripts are used for solution verification and error analysis.

Techniques and verification: Position solutions are evaluated based on convergence behavior, residual errors, and horizontal positioning accuracy.

Key outputs: Stable PVT solution with acceptable horizontal error performance and consistent time estimates.

Accomplishment until now: RTKLIB linearization based PVT solver block successfully configured and integrated to GNSS SDR and validated over clear and noisy synthetic data. It is planned to be fine tuned to achieve higher timing efficiency.

4.2.1.6 GUI Design and System Integration

The GUI Design and System Integration phase focuses on combining all GNSS processing modules - acquisition, tracking, telemetry decoding, and PVT into a single functional workflow and providing a simple interface for real-time visualization. Since this is the final stage of the project and depends on earlier modules being fully validated, the current work mainly involves defining the GUI structure and establishing data connections with GNSS-SDR rather than implementing the full interface. The planned GUI will be developed in Python and will visualize key system outputs such as estimated C/N₀ values, the number of tracked satellites, a basic satellite skyplot, and the receiver's computed position at 1 Hz, in accordance with GUI-R-1 to GUI-R-4. Table 13 details the GUI focused risks and the respective mitigation strategies.

Table 13: GUI focused Risks, Impacts and Mitigation solutions

Risk	Impact	Mitigation
Data format mismatch between GNSS-SDR and GUI	Incorrect C/N ₀ or satellite display	Standardize output format (JSON/CSV)
GUI refresh delay or slow rendering	Lag in constellation/position updates	Use lightweight plotting and 1 Hz updates
GUI crash under unexpected values (e.g., 0 satellites)	Loss of visualization	Add basic exception handling

Strategy: The strategy for GUI design corresponding to WP6 is to integrate all receiver modules into a single end-to-end pipeline and provide real-time visualization of system outputs.

Tools and software: A PyQt based GNSS SDR Monitor, GUI framework is used to display C/N₀ values, satellite count, constellation view, and real-time position updates.

Techniques and verification: End-to-end system operation is verified after acquisition, tracking, and PVT modules are validated individually).

Key outputs: A fully integrated GNSS SDR receiver with real-time visualization and user-level monitoring capability.

Accomplishment until now: Custom GNSS SDR Monitor GUI base design is completed and validated over clear and noisy synthetic data.

4.2.2 Progress and the Current State

4.2.2.1 Progress up to CM1

Figure 14, 15 and 16 illustrates an attempt until CM1 to simulate certain algorithms discussed in previous section on already available raw data:

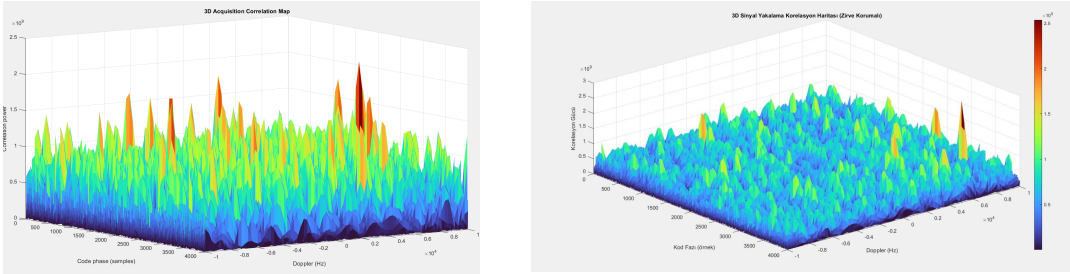


Figure 14: Generated PCPS Plot and PSD Analysis of Pre-Recorded Data

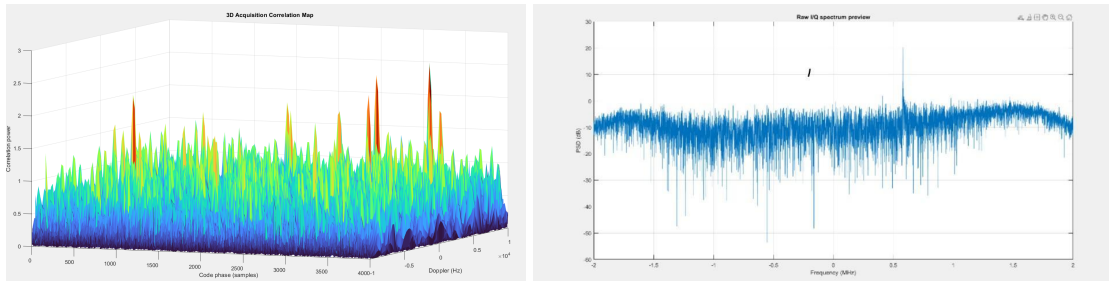


Figure 15: Generated PCPS Plot and PSD Analysis of Pre-Recorded Data



Figure 16: Generated PVT Solutions using GNSS SDR.

The CM1 progress of the project can be explained in terms of literature review on SDR devices, geolocation/navigation methodologies, GNSS signal structures and processing, and specifically GPS L1 and L2 signal structures and signal processing chains. The GNU Radio software and GNSS SDR software were set up and started to be used. Additionally, MATLAB simulations over acquisition were performed using pre-recorded baseband data, whose results are shown in the figures above. Figure 17 summarizes our progress until CM1:

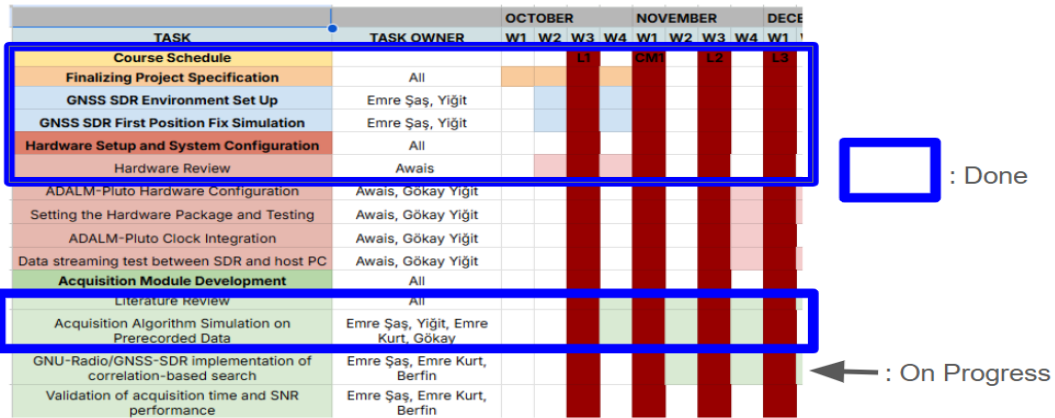


Figure 17: Progress until CM1 (14.11.2025) on Gantt Chart

4.2.2.2 Progress up to CM2

The progress up to CM2 can be explained in terms of three phases, the tracking simulation on Matlab, Synthetic data generation and custom GUI beside tracking literature review.

4.2.2.2.1 Synthetic Data Generation

To generate synthetic data GPS SDR SIM software was used. As there were no accessible prerecorded baseband raw GNSS data the focus on the simulation changed to run over synthetic data rather than pre recorded data. The synthetic data includes a software generated GNSS raw baseband signal that is for a given specific location. It resembles what the SDR would sample if it recorded the GNSS signal in the given specific location. To generate the synthetic data it must be fed with both the coordinate for the sampling to be simulated and the ephemeris file for a specific GNSS satellite provider. The ephemeris file includes the constellation of the broadcasting GNSS satellites and their specific broadcasting information such as PRN numbers, telemetry data and their velocities causing the code phase shift and doppler shift in carrier frequencies. Then using those data a specific synthetic baseband sampled GNSS data can be generated for a given coordinate.

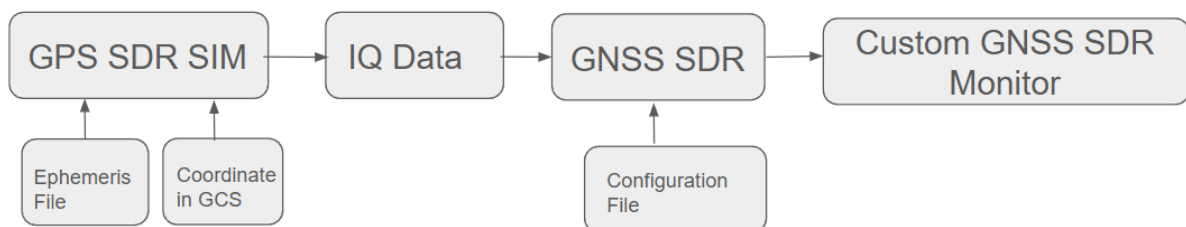


Figure 18: Synthetic data Generation and Simulation Structure

The synthetic data for Bilkent University EE building was generated for simulation. The results of clean and noisy synthetic data simulation on the custom GUI would be discussed in the subsequent sections. The results come out as compatible with the expectation that the noisy data results in a lower carrier to noise ratio. Hence, the signal receiver chain must guarantee low noise to successfully decode the telemetry data.

4.2.2.2.2 Tracking Matlab Simulation

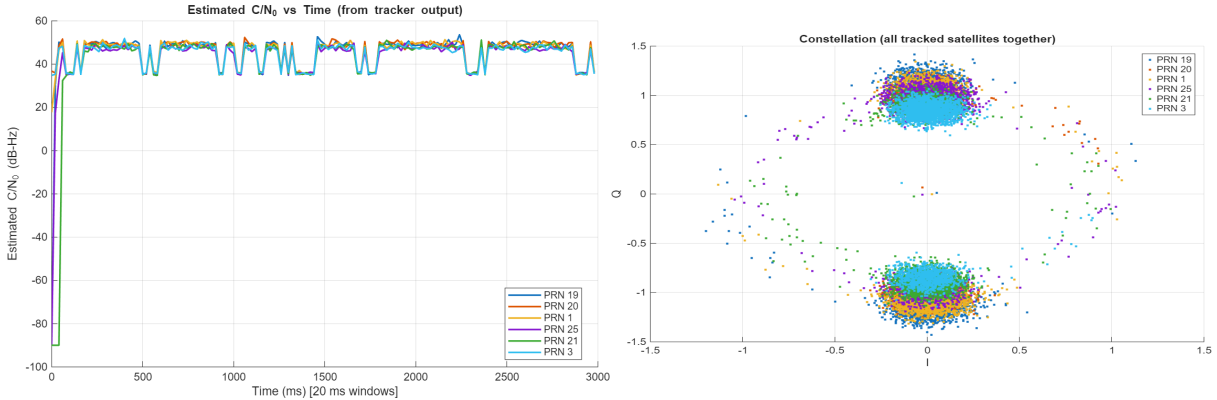


Figure 19: Tracking Matlab Simulation: Resulting IQ constellation and C/N_₀ results

The Tracking part is an essential part of GNSS signal processing chain as it makes inphase and quadrature demodulation and telemetry decoding possible by tracking the acquired satellite's code phase shift and carrier frequency doppler shift. Hence, the DLL and FLL based tracking loop algorithm tested in Matlab using synthetic data. After tracking convergence, the estimated C/N_₀ stabilizes around 45–50 dB-Hz, indicating reliable carrier and code lock, while short-term drops are mainly caused by navigation data bit transitions and residual carrier phase errors.

4.2.2.2.3 GNSS-SDR Monitoring GUI Extension and Preliminary Performance Demonstration

As part of the project, and to comply with the feedback of our assigned Teaching Assistant, the development of a real-time graphical user interface (GUI) was initiated to monitor and analyze the outputs of the GNSS-SDR receiver. The primary objective of this GUI is to provide continuous visibility into navigation performance, solution quality, and estimation uncertainty during receiver operation.

4.2.2.2.3.1 Extension of the Baseline GNSS-SDR Monitor GUI

To begin with, the graphical user interface (GUI) already developed by the GNSS-SDR open-source community was extended to support enhanced navigation performance monitoring and uncertainty-aware analysis [12]. The baseline GNSS-SDR Monitor provides real-time visualization of receiver status through serialized Monitor and PVT data streams; however, its primary focus is operational monitoring rather than quantitative evaluation of navigation accuracy.

Our extended GUI builds upon this existing infrastructure without modifying the GNSS-SDR core. New visualization components and data-handling logic were introduced at the GUI level to enable time-consistent monitoring of navigation solutions, quality indicators, and uncertainty-related metrics. This approach preserves compatibility with standard GNSS-SDR configurations while allowing advanced analysis capabilities to be added in a modular and non-intrusive manner. Figure 20 shows the general layout of our designed GUI.

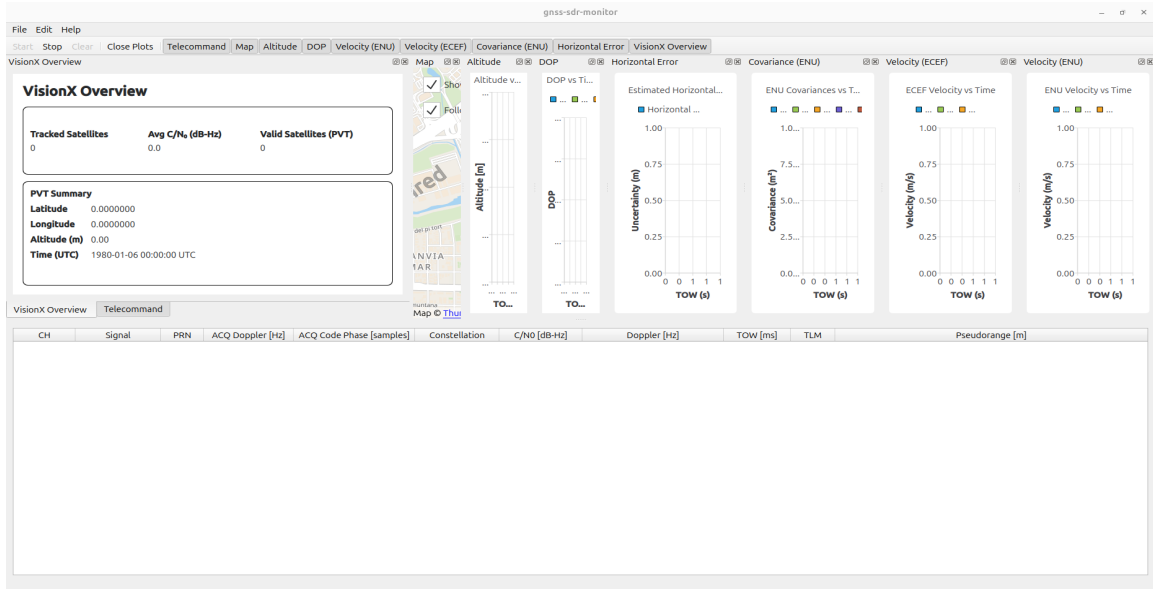


Figure 20: Extended GNSS-SDR Monitor GUI main window

4.2.2.2.3.2 Communication Setup and GNSS-SDR Configuration

In order to realize reliable communication between GNSS-SDR and the monitoring GUI, we need serialized data streams to be transmitted over User Datagram Protocol (UDP), along with an optional Transmission Control Protocol (TCP) based telecommand interface, which is essentially controlling GNSS-SDR through GUI commands. However, since the telecommand interface is outside the scope of our project, we restrict ourselves, for now, to use this utility. Note that the proper configuration of IP addresses and port numbers on both the receiver and GUI sides is critical for successful data exchange.

Two independent UDP streams are used: i) **PVT block stream**, which provides navigation solution outputs such as Time of the Week (TOW), position, velocity, number of valid satellites, and covariance data. ii) **Monitor block stream**, which provides internal receiver status information related to acquisition and tracking stages. Figure 21 represents these data streams from the GNSS-SDR modular structure.

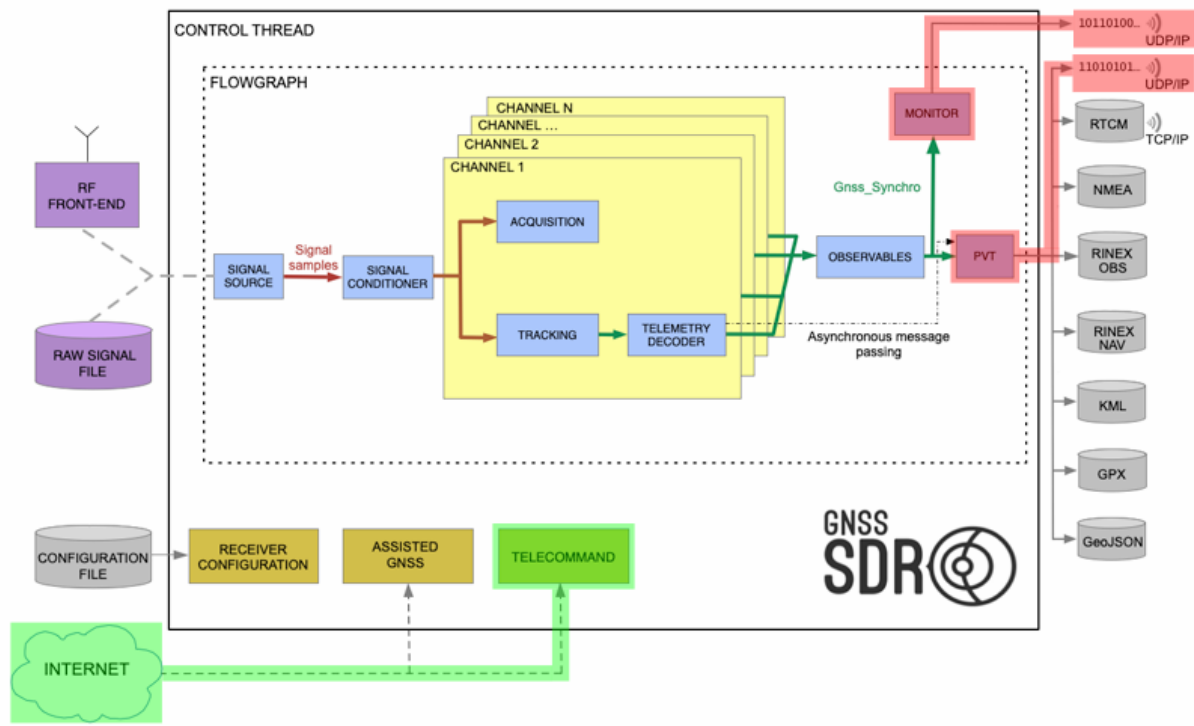


Figure 21: The Monitor block streaming and the PVT block streaming are distinctly indicated in red, while the Telecommand module is highlighted in green (restricted for now).

Now, by default, GNSS-SDR offers several navigation- and status-related parameters through its serialized PVT and Monitor Block streams. These parameters include timing information, navigation state estimates, uncertainty measures, dilution of precision metrics, satellite statistics, and solution quality indicators. Table 14 which shows the full set of navigation-related parameters available from the GNSS-SDR PVT Block for custom streaming, can be found in Appendix F.

In the GNSS-SDR configuration file, the PVT block stream is enabled by specifying the destination IP address and UDP port corresponding to the machine running the GUI, as shown in Figure 22 (i). For local operation, the loopback address (127.0.0.1) is used, while remote monitoring can be achieved by specifying the appropriate network address.

```
PVT.enable_monitor=true
PVT.monitor_client_addresses=127.0.0.1
PVT.monitor_udp_port=1111
```

```
Monitor.enable_monitor=true
Monitor.decimation_factor=1
Monitor.client_addresses=127.0.0.1
Monitor.udp_port=1112
```

Figure 22 (i) (left) and (ii) (right): GNSS-SDR configuration file: PVT Block stream settings (left) and Monitor Block Stream Settings (right)

Similarly, the Monitor block stream is enabled by assigning a matching IP address and UDP port. The decimation factor is configured to control the update rate of monitoring data. The settings are shown in Figure 22 (ii).

On the GUI side, the same port numbers are configured through the preferences menu, as shown in Figure 23. Ensuring exact correspondence between the GNSS-SDR configuration file and the GUI settings is essential; any mismatch prevents the GUI from receiving data streams correctly.

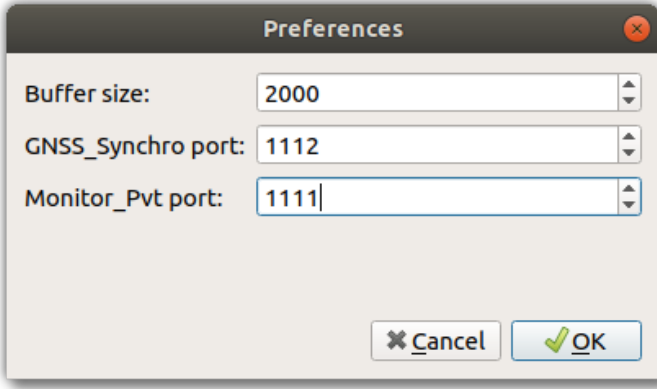


Figure 23: GUI preferences panel showing configured port numbers

4.2.2.2.3.3 Implemented GUI Components, Parameter Selection, and Visualization Strategy

Given the wide range of parameters available through the GNSS-SDR PVT stream, a selection strategy was adopted to identify quantities that are most relevant for navigation performance evaluation and uncertainty analysis. Accordingly, the current version of the GUI focuses on a subset of parameters including position components, velocity components, covariance elements associated with position uncertainty, and the number of valid satellites. This selection ensures that the most informative navigation-level indicators are visualized while maintaining clarity and responsiveness in real-time operation.

In addition to the PVT stream, the GNSS-SDR Monitor stream is utilized to provide per-channel signal-level diagnostics that support interpretation of the navigation solution. Although these parameters do not directly represent positioning accuracy, they offer critical analysis into tracking stability and measurement reliability. The GUI therefore integrates selected Monitor stream outputs, allowing per-channel inspection indexed by channel number and PRN. These include in-phase (I) and quadrature (Q) signal components for constellation visualization, Doppler frequency estimates to observe carrier dynamics, carrier-to-noise density ratio (C/N_0) as an indicator of signal quality, and pseudorange measurements representing the raw observables used by the navigation filter.

All selected parameters are visualized using time-consistent plotting mechanisms referenced to GNSS Time of Week (TOW), ensuring synchronization across navigation- and signal-level indicators. This layered visualization approach enables

navigation accuracy and uncertainty metrics to be interpreted in the context of underlying signal conditions and satellite availability.

4.2.2.2.3.4 GUI Functionality with Synthetic Dataset Simulation

To demonstrate the functionality of the implemented visualization framework, an initial simulation was conducted using a synthetic GNSS dataset. Estimated receiver positions obtained from the PVT stream were visualized both as time series and on a map-based interface. The map visualization provides an intuitive spatial representation of receiver behavior and complements the numerical plots by highlighting trajectory consistency and spatial dispersion under controlled conditions. The same visualization pipeline is directly applicable to real GNSS-SDR data without modification. Table 15 summarizes the results of simulation on our GUI with relevant figures found in Appendix G.

Table 15: Results obtained on GUI through Synthetic Dataset Simulation

Title	Appendix G	Explanation
VisionX Overview Panel	Figure 24	The overview panel confirms correct end-to-end operation of the GNSS-SDR-GUI pipeline. In the synthetic run, 8 satellites are tracked and 7 contribute to the PVT solution, with an average $C/N_0 \approx 52 \text{ dB} - \text{Hz}$, indicating strong signal conditions. Sufficient satellite availability and high C/N_0 ensure observability of the navigation states and stable filter convergence.
Per-Channel Monitor Table	Figure 25	The per-channel table presents signal-level observables indexed by channel and PRN. C/N_0 values in the range of $\approx 49\text{--}58 \text{ dB} - \text{Hz}$ and Doppler estimates around $\pm 2.5\text{--}3.6 \text{ kHz}$ indicate robust carrier tracking. Pseudoranges on the order of $2 \times 10^7 \text{ m}$ confirm valid code measurements feeding the navigation filter.
I/Q Constellation Diagrams	Figure 26	The constellation plots show compact clustering of prompt I/Q samples, characteristic of stable phase and code lock. Such clustering indicates low phase jitter and correct carrier wipe-off, which is a prerequisite for reliable pseudorange and Doppler estimation.
C/N_0 vs Time	Figure 27	C/N_0 remains stable within a $2\text{--}4 \text{ dB} - \text{Hz}$ band around $50\text{--}55 \text{ dB} - \text{Hz}$, reflecting steady received signal power in the synthetic scenario. Small fluctuations are attributable to tracking loop

Title	Appendix G	Explanation
		dynamics rather than signal fading, supporting consistent measurement quality over time.
Doppler Frequency vs Time	Figure 28	Doppler estimates exhibit smooth temporal evolution with bounded variations of tens of hertz. This behavior is consistent with a well-tuned frequency-locked loop tracking the relative satellite-receiver motion defined by the simulation, without loss-of-lock or cycle slips.
Map-Based Position Visualization	Figure 29	The map view shows a tight cluster of estimated positions around a fixed location, as expected in a static synthetic scenario. The spatial dispersion is limited to a few meters, aligning with the covariance-based horizontal uncertainty and indicating good horizontal solution stability.
Altitude vs Time	Figure 30	Altitude estimates fluctuate around $\approx 1041\text{ m}$ with small periodic variations. Vertical positioning typically exhibits higher noise due to satellite geometry, and the bounded nature of these variations indicates a stable but geometry-limited vertical solution.
Horizontal Position Uncertainty (1σ)	Figure 31	The estimated horizontal uncertainty increases smoothly from $\approx 3.07\text{ m}$ to $\approx 3.08\text{ m}$, indicating that the navigation filter has converged and that uncertainty evolution is dominated by geometry rather than transient effects. This output directly reflects the covariance reported by the estimator.
ENU Covariance Components	Figure 32	The ENU covariance plot shows diagonal terms on the order of $10^0 - 10^1\text{ m}^2$, while cross-covariance terms remain much smaller. This structure implies weak coupling between horizontal and vertical states and a well-conditioned estimation problem.
ENU Velocity vs Time	Figure 33	ENU velocity components fluctuate around zero with magnitudes below $\pm 1\text{ m/s}$, consistent with a static receiver scenario. The noise-like behavior reflects measurement uncertainty rather than physical motion, confirming consistency between the simulated dynamics and estimated states.

The simulation was also repeated for noisy dataset, as found in Figure 34 in Appendix G. It was observed that the C/N₀ was lower.

4.2.3 Future Plans

The plans for the project can be explained in Hardware integration and signal processing terms. All the hardware packs that consist of active antenna, active antenna supply, bias tee and DC block for inter connections of antenna supply amplified RF band signal and Adalm-Pluto SDR will be integrated and set up. Additionally, the reference clock of the Adalm-Pluto SDR will be replaced by a more stable oscillator. Moreover, after the hardware pack integration functionality of the pack will be validated. In terms of GNSS signal processing software, the prerecorded data processing structure used in GNSS SDR will be adapted to real time samples acquired by Pluto SDR. Additionally, some accelerating algorithms and estimation methodologies will be researched and possibly adapted to the signal processing chain to improve the time efficiency and solution accuracy of the system.

4.2.3.1 Validation and Precaution via Gpredict

Since there may be some unexpected and hidden errors during the TCXO integration process or in the RF pipeline, an outer validation strategy is needed since testing the system with itself is not reliable. To verify that the external TCXO mitigates the risk related to stability, and the RF pipeline is healthy, software-based validation strategy will be used by utilizing the app Gpredict [21]. Gpredict is a real-time satellite tracking and orbit prediction application which uses updated TLE data and the standard NORAD SGP4 [22]. Gpredict shows the real-time and future parameters of the satellites. In this project, Gpredict is not only used to validate results ,but also to optimize the field test.

Before starting to collect data, it is beneficial to know which satellites will exhibit high elevation angles (indicator of satellite being directly above the test field), long pass durations (for consistency over the test durations) and clear line of sight conditions during the test process, and Gpredict allows us with these critical information.Being able to select the optimal scenarios, reduces the external errors and therefore allows us to track the behaviour of the hardware performance.

After deciding the test date, the theoretical satellite kinematic parameters are found by using Gpredict. One of the most important parameters is the range rate (relative radial velocity) between the receiver and the satellite. To calculate the Doppler shift below formula is used:

$$\Delta F = \text{Doppler shift}, V_r = \text{Range Rate}, F_c = \text{Carrier Frequency}, c = \text{Speed of Light}.$$

$$\Delta F = - (V_r \times F_c) \div c. \quad [23]$$

Calculated Doppler profiles for each satellite will be compared with the Doppler estimates produced by GNSS-SDR. On top of doppler verification,several helpful parameters provided by Gpredict are used to validate the data. Specifically, visibility, signal loss, and AOS/LOS (Acquisition/Loss of Signal) information are used

to validate that observed tracking behavior is consistent .Sudden loss of lock or irregular Doppler behavior is cross-checked against predicted visibility intervals to distinguish hardware- or signal-related issues from natural pass termination effects.

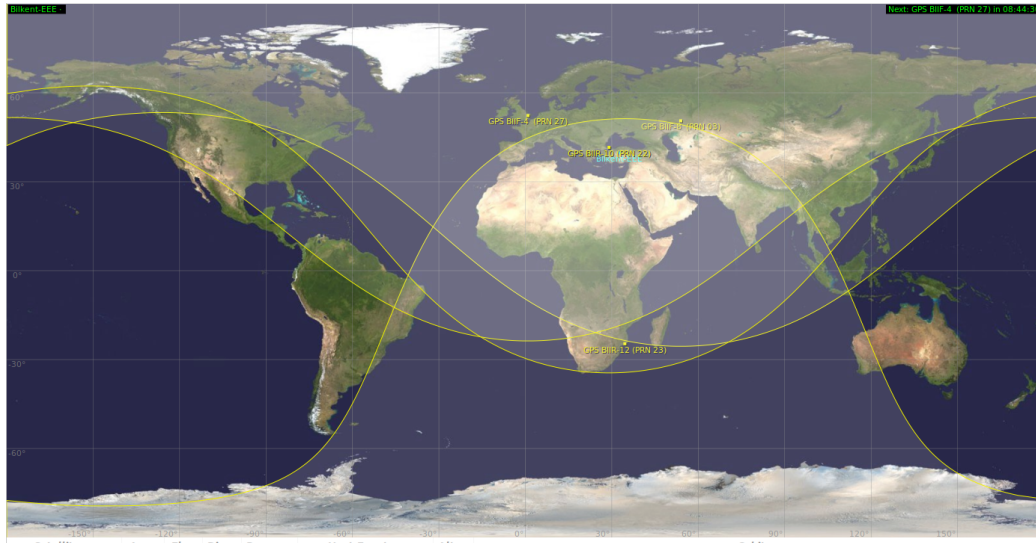


Figure 35: Gpredict Map Interface showing 3 example satellites and their trajectory (yellow dots) and the current added position of EE-Building (Blue Dot)



Figure 36: Selected Parameters (Choices Are Given In The Figure 37) Shown In The terminal.

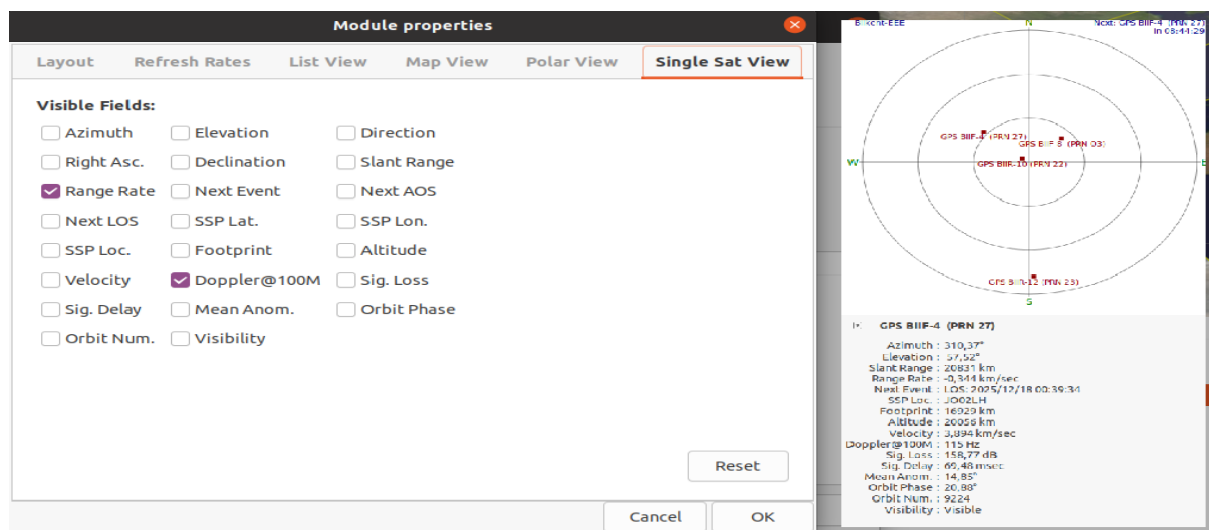


Figure 37: Parameters Accessible On The Left and Constellation and Parameters Related To Closest Satellite On The Right

4.2.3.2 Planned Horizontal Positioning Error and Uncertainty Analysis

4.2.3.2.1 Reference-Based Horizontal Error Definition (Planned)

To evaluate the horizontal positioning performance of the GNSS-SDR receiver, a reference-based error analysis will be conducted using known ground-truth coordinates. A fixed reference position will be assumed for static receiver experiments, enabling direct comparison between estimated and true positions.

The receiver position estimates obtained from the PVT solution will first be transformed into a local tangent plane coordinate system, expressed in East (E), North (N), and Up (U) components. Horizontal positioning error will be defined using only the East and North components, using 2D - Distance Root Mean Square (DRMS) as its a practical navigation accuracy assessment for our project's scope. Table 16 which shows several position accuracy metrics for 2D and 3D positioning, expressed in a local ENU reference frame, can be found in Appendix H [24].

For each epoch l , the local horizontal errors will be computed as:

$$e[l] = E[l] - E_{ref}$$

$$n[l] = N[l] - N_{ref}$$

where E_{ref} and N_{ref} denote the reference East and North coordinates, respectively.

Using a total of L valid position estimates, the static empirical standard deviations of the horizontal error components will be calculated as:

$$\sigma_E = \sqrt{\frac{1}{L-1} \sum_{l=1}^L e[l]^2}, \quad \sigma_N = \sqrt{\frac{1}{L-1} \sum_{l=1}^L n[l]^2}$$

Afterwards, based on these quantities, the empirical DRMS metric will be computed as:

$$DRMS_{emp} = \sqrt{\sigma_E^2 + \sigma_N^2} = \sqrt{\frac{1}{L-1} \sum_{l=1}^L (e[l]^2 + n[l]^2)}$$

This metric represents the radius of a circle centered at the true receiver position that is expected to contain approximately 65% of the horizontal position estimates under Gaussian error assumptions.

4.2.3.2.2 Covariance-Based DRMS Estimation (Planned)

In addition to empirical error analysis, the internal uncertainty estimates reported by the GNSS-SDR navigation filter/estimator will be evaluated. Note that we made sure to display these covariances on the GUI monitor for easy analysis. The PVT block outputs a position covariance matrix expressed in the Earth-Centered Earth-Fixed (ECEF) coordinate frame.

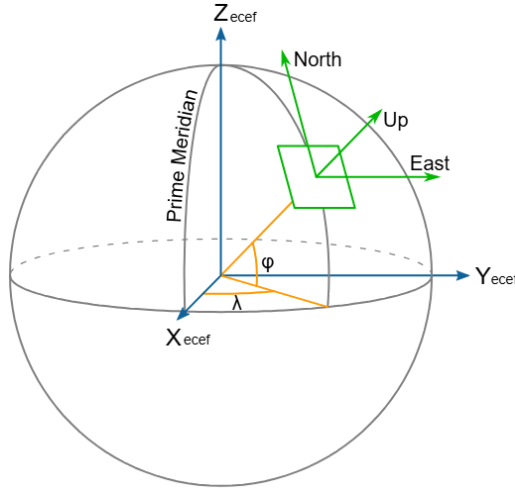


Figure 38: Illustration of ECEF versus ENU Coordinate Frameworks [25]

To enable comparison with reference-based horizontal errors, the ECEF covariance matrix will be transformed into the local ENU frame using a rotation matrix defined at the reference latitude φ and longitude λ :

$$P_{ENU} = R_{ECEF \rightarrow ENU} P_{ECEF} R_{ECEF \rightarrow ENU}^T$$

The rotation matrix is given by:

$$R_{ECEF \rightarrow ENU} = \begin{bmatrix} -\sin\lambda & \cos\lambda & 0 \\ -\sin\varphi\cos\lambda & -\sin\varphi\sin\lambda & \cos\varphi \\ \cos\varphi\cos\lambda & \cos\varphi\sin\lambda & \sin\varphi \end{bmatrix}$$

From the transformed covariance matrix, the horizontal uncertainty will be extracted from the diagonal elements corresponding to the East and North components. The predicted DRMS value will then be computed as:

$$DRMS_{pred} = \sqrt{P_{EE} + P_{NN}}$$

This quantity represents the model-based estimate of horizontal positioning uncertainty, reflecting the confidence level reported internally by the navigation filter/estimator.

4.2.3.2.3 Planned Calibration and Consistency Assessment

To assess the consistency between the predicted uncertainty and the observed positioning accuracy, a calibration analysis will be performed by comparing empirical and covariance-based DRMS values.

A calibration ratio will be defined as:

$$\gamma = \frac{DRMS_{emp}}{DRMS_{pred}}$$

This ratio will be used to evaluate the quality of the navigation filter's uncertainty modeling according to the following interpretation:

Table 17: Calibration Ratios and their Implications

Ratio Value	Estimator Status	Description
$\gamma \approx 1$	Well-Calibrated	Predicted Uncertainty matches the actual error.
$\gamma > 1$	Over-confident	Errors are larger than predicted uncertainty.
$\gamma < 1$	Conservative	Uncertainty is overestimated.

Deviations between empirical accuracy and predicted uncertainty will be investigated in relation to satellite geometry, convergence behavior, and measurement conditions. We intend to visualize the analysis results through the extended monitoring GUI, enabling real-time comparison between actual positioning accuracy and predicted uncertainty during receiver operation.

5. INITIAL PLAN FOR FINAL DEMO

In order to assess receiver performance under practical operating conditions, the ADALM-Pluto SDR will be used in the final demonstration to acquire real-time GPS L1 and L2 signals at the Bilkent University campus and at randomly chosen outdoor locations in Ankara. The full end-to-end functionality of the suggested system will be demonstrated by streaming the received RF signals to the host computer and processing them in real time using the GNSS-SDR software chain.

The demo will start with the activation and validation of the hardware front-end with the external TCXO is embedded. Once the RF stream is initiated and it is checked, ADALM-Pluto will start the real-time acquisition process, and correlation peaks corresponding to visible satellites will be observed, confirming the detection of live GNSS signals.

Tracking and navigation stages will follow the acquisition part, where ACQFR1, TRKFR1, and PVTFR1 functional requirements will be directly assessed using real-time measurements. Loop performances will be checked by observing the parameters such as carrier-to-noise density ratio (C/N_0), Doppler frequency estimates, and lock status via the developed GUI.

To validate the results mentioned above, parameters will be cross checked with the predicted satellite visibility and Doppler information provided by Gpredict. This comparison will serve as an external reference to verify frequency stability, Doppler estimation accuracy, and overall receiver reliability.

In the final stage of the demo, PVT solutions will be presented in real time and in a neat format. Estimated position solution will both be shown on map and in coordinates. Key performance metrics such as execution time, position accuracy, start up delay will be shown.

6. DETAILED EQUIPMENT LIST

Table 18: Detailed equipment list and costs [26]

Product	Price (EUR)	Way To Obtain
ADI Adalm Pluto SDR REV C	233.25	By Purchase
U-blox ANN-MB2-00	63.47	By Purchase
Mini-Circuits ZFBT-4R2G+ Bias Tee	80.60	By Purchase
Mini-Circuits BLK-89-S+	20.91	By Purchase
Epson TG2520SMN Temperature-Compensated Crystal Oscillator	2.98	By Purchase
Total Price	401.21	

7. REFERENCES

- [1] European Space Agency (ESA), *Navipedia Main Page*. ESA GSSC Navipedia, 2025. [Online]. Available: https://gssc.esa.int/navipedia/index.php/Main_Page [Accessed: 13 Nov. 2025].
- [2] Analog Devices, Inc., *ADALM-PLUTO SDR Active Learning Module—Product Highlight*, Rev. A, Norwood, MA, USA, 2017. [Online]. Available: <https://www.analog.com/en/design-center/evaluation-hardware-and-software/evaluation-boards-kits/adalm-pluto.html>
- [3] Huace Microelectronics (HMuSRP), *Products*. [Online]. Available: https://www.hmusrp.com/products/?gad_source=1&gad_campaignid=21734890059 [Accessed: 28 Sep. 2025].
- [4] B. M. Ledvina, M. L. Psiaki, S. P. Powell, and P. M. Kintner, Jr., “Real-time software receiver,” U.S. Patent 7,010,060, Mar. 7, 2006.
- [5] B. M. Ledvina, M. L. Psiaki, S. P. Powell, and P. M. Kintner, Jr., “Real-time software receiver,” U.S. Patent 7,305,021, Dec. 4, 2007.
- [6] K. Van Dierendonck, M. Xu, and P. L. Kazemi, “System, method, and computer program for a low power and low cost GNSS receiver,” U.S. Patent 9,116,234, Aug. 25, 2015.
- [7] u-blox AG, *ANN-MB2 L1/L2/L5/E6/B3/L All-Band High-Precision GNSS Antenna—Data Sheet*, Document UBX-DOC-963802114-12775, Thalwil, Switzerland, Feb. 2025. [Online]. Available: <https://www.u-blox.com/en/product/ann-mb-series>
- [8] Mini-Circuits, *ZFBT-4R2G+ Coaxial Bias-Tee (10–4200 MHz)*, Data Sheet, Rev. D, Brooklyn, NY, USA, 2024. [Online]. Available: <https://www.minicircuits.com/WebStore/dashboard.html?model=ZFBT-4R2G%2B>
- [9] Mini-Circuits, *BLK-89-S+ Coaxial DC Block (0.1–8000 MHz)*, Data Sheet, Rev. G, Brooklyn, NY, USA, 2024. [Online]. Available: <https://www.minicircuits.com/WebStore/dashboard.html?model=BLK-89-S%2B>
- [10] Seiko Epson Corporation, *TG2520SMN Temperature-Compensated Crystal Oscillator (TCXO) Full Data Sheet*, Spec. No. TG2016/2520SMN_EN Ver. 2.0, Tokyo, Japan, 2025. [Online]. Available: <https://www.epsondevice.com/crystal/en/products/crystal-oscillator/tg2520smn.html>
- [11] C. Fernandez, “GNSS-SDR,” *GitHub*. (Online). Available: <https://github.com/carlesfernandez/gnss-sdr?tab=readme-ov-file>. [Accessed: Nov. 24, 2025].

- [12] A. Cebrián-Juan, “gnss-sdr-monitor,” GitHub repository, 2020. [Online]. Available:
<https://github.com/acebrianjuan/gnss-sdr-monitor>. [Accessed: Nov. 24, 2025].
- [13] GNSS-SDR, “Custom Streaming,” *GNSS-SDR website*. (Online). Available:
<https://gnss-sdr.org/docs/sp-blocks/pvt/#custom-streaming>. [Accessed: Nov. 24, 2025].
- [14] u-blox AG, “GNSS Antennas—An Introduction to Bandwidth, Gain Pattern, and Polarization,” Application Note UBX-15030289, Rev. 1.01, Thalwil, Switzerland, Apr. 2016. [Online]. Available:
https://content.u-blox.com/sites/default/files/products/documents/GNSS-Antennas_AppNote_%28UBX-15030289%29.pdf
- [15] R. Khan, S. U. Khan, R. Zaheer, and S. Khan, “Acquisition strategies of GNSS receiver,” in *Proc. Int. Conf. Computer Networks and Information Technology (ICCNIT)*, Jul. 2011, pp. 119–124, doi: 10.1109/ICCNIT.2011.6020917.
- [16] Q. Lei and L. Lei, “GPS signal acquisition based on FFT,” in *Proc. 2nd Int. Conf. Information Technology and Computer Science (ITCS)*, 2010, pp. 110–113, doi: 10.1109/ITCS.2010.33.
- [17] S. Cui, D. Wang, B. Holtkamp, X. Yao, T. Chi, and J. Fang, “A multi-frequency acquisition algorithm for a GNSS software receiver,” in *Proc. IEEE Int. Geosci. Remote Sens. Symp. (IGARSS)*, Jul. 2018, doi: 10.1109/IGARSS.2018.8517898.
- [18] M. Foucras, B. Ekambi, F. Bacard, O. Julien, and C. Macabiau, “Assessing the performance of GNSS signal acquisition: new signals and GPS L1 C/A code,” *Inside GNSS*, Jul./Aug. 2014, pp. 68–76. [Online]. Available:
<https://insidegnss.com/assessing-the-performance-of-gnss-signal-acquisition/>. [Accessed: 13 Nov. 2025].
- [19] A. Albu-Rghaif, H. Y. Radhi, and R. G. Dawood, “Combining GPS and Galileo signals acquisition in a single processing chain,” *Diyala Journal of Engineering Sciences*, pp. 157–167, Dec. 2024, doi: 10.24237/djes.2024.17409.
- [20] M. Andrianarison and G. Macabiau, “New approach of high-sensitivity techniques using GNSS mass-market receivers,” *Sensors*, vol. 18, no. 11, 3690, 2018, doi: 10.3390/s18113690.
- [21] “Gpredict: Free, Real-Time Satellite Tracking and Orbit Prediction Software,” [oz9aec.dk](https://oz9aec.dk/gpredict/). <https://oz9aec.dk/gpredict/>
- [22] G. Acciarini, A. G. Baydin, and D. Izzo, “Closing the gap between SGP4 and high-precision propagation via differentiable programming,” *Acta Astronautica*, vol. 226, pp. 694–701, Nov. 2024, doi: <https://doi.org/10.1016/j.actaastro.2024.10.063>.

- [23] A. Angrisano, G. Cappello, S. Gaglione, and C. Gioia, “Velocity Estimation Using Time-Differenced Carrier Phase and Doppler Shift with Different Grades of Devices: From Smartphones to Professional Receivers,” *Algorithms*, vol. 17, no. 1, pp. 2–2, Dec. 2023, doi: <https://doi.org/10.3390/a17010002>.
- [24] “Accuracy,” GNSS-SDR, 2025. [Online]. Available: <https://gnss-sdr.org/design-forces/accuracy/>. [Accessed: Dec. 15, 2025].
- [25] “Local tangent plane coordinates,” Wikipedia, Nov. 18, 2025. [Online]. Available: https://en.wikipedia.org/wiki/Local_tangent_plane_coordinates. [Accessed: Dec. 15, 2025].
- [26] “visionx Edit Project – Pricing Table,” Mouser Electronics Europe, 2025. [Online]. Available: <https://eu.mouser.com/Tools/Project/Share?AccessID=0fa2b251df> (accessed Dec. 27, 2025)

8. APPENDICES

Appendix A - Overall System Architecture

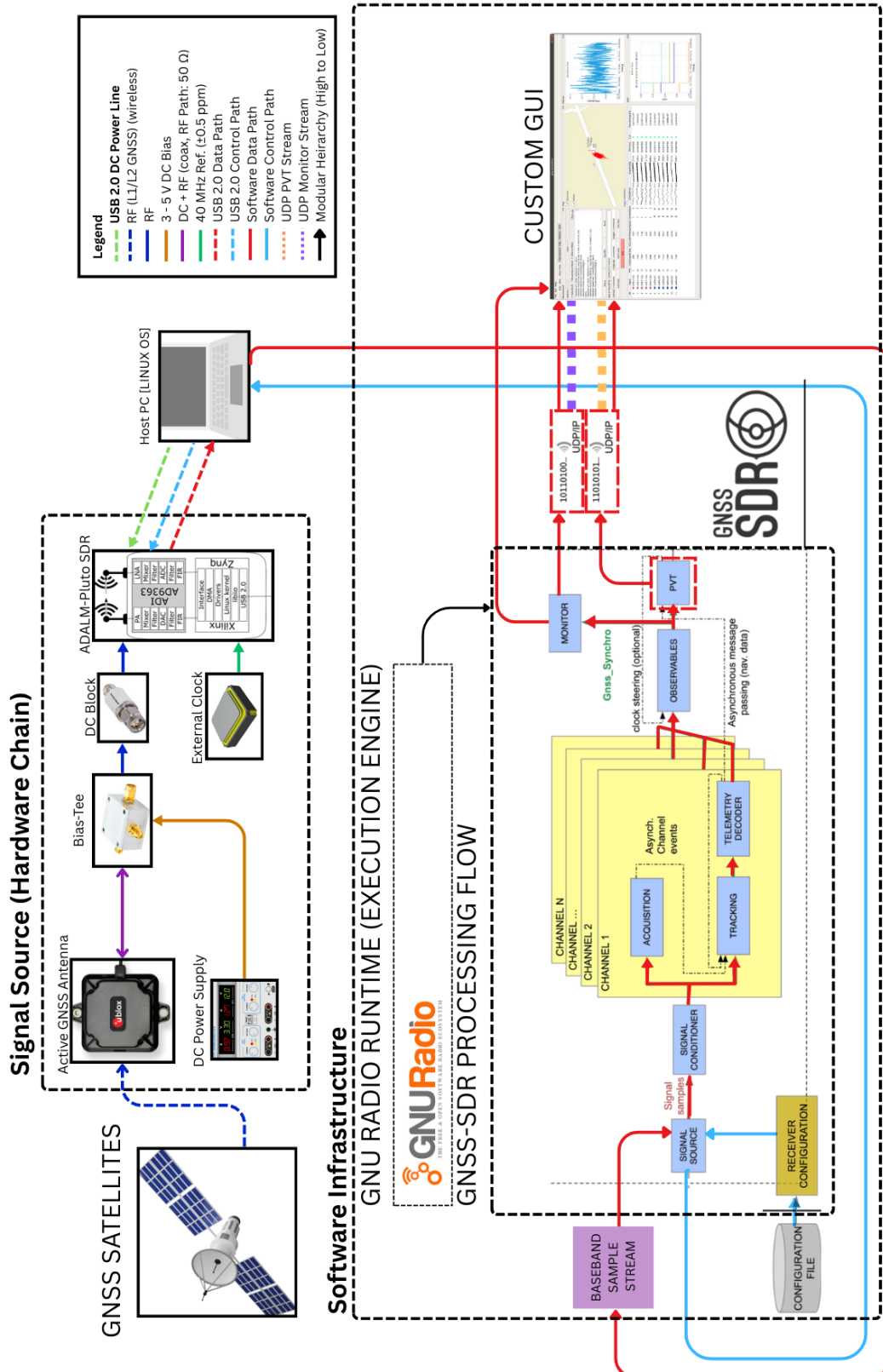


Figure 2: Overall System Architecture [2], [7], [8], [9], [10], [11], [12], [13].

Appendix B - Work Breakdown Structure

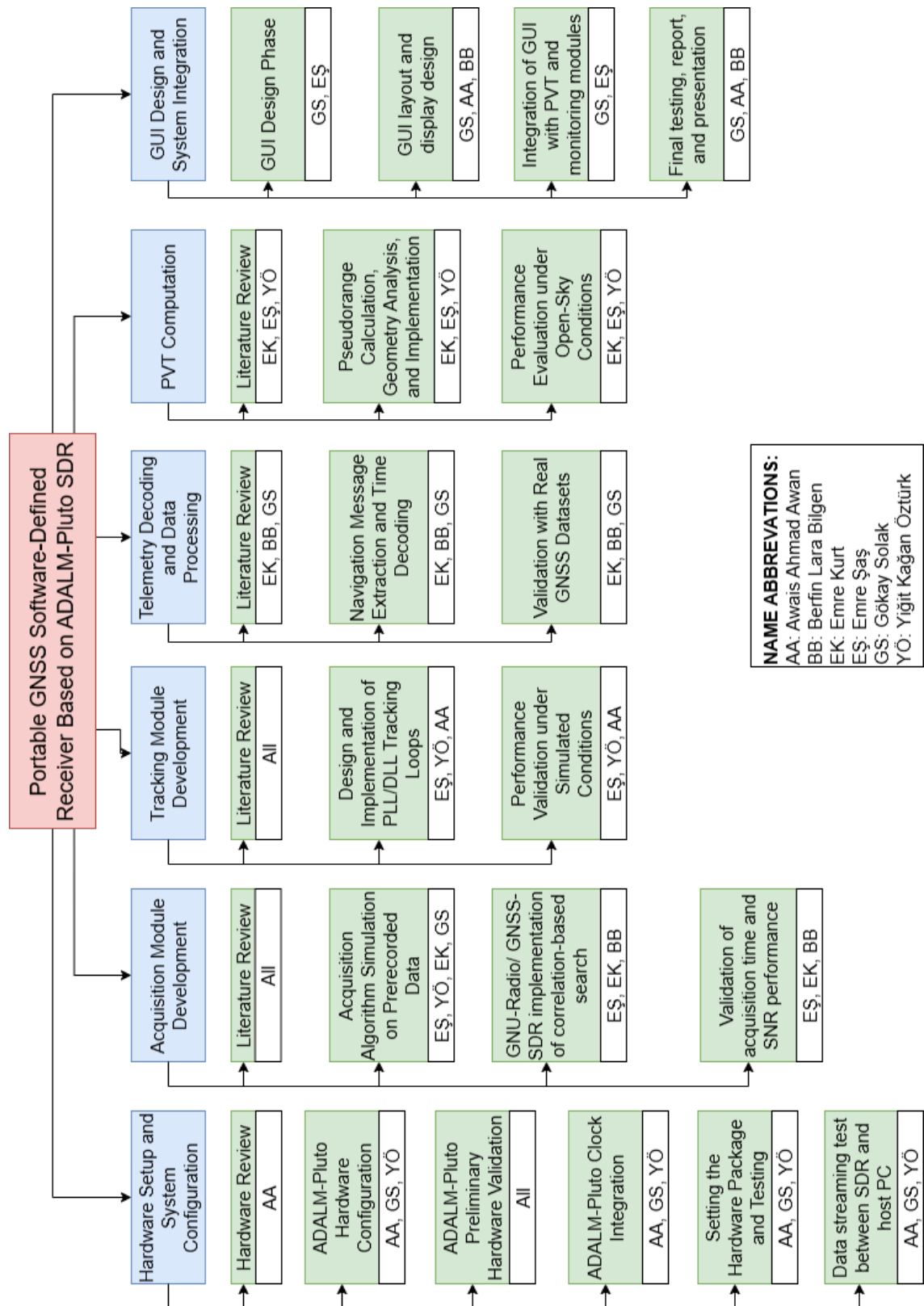


Figure 3: Work Breakdown Structure

Appendix C - Project Timeline

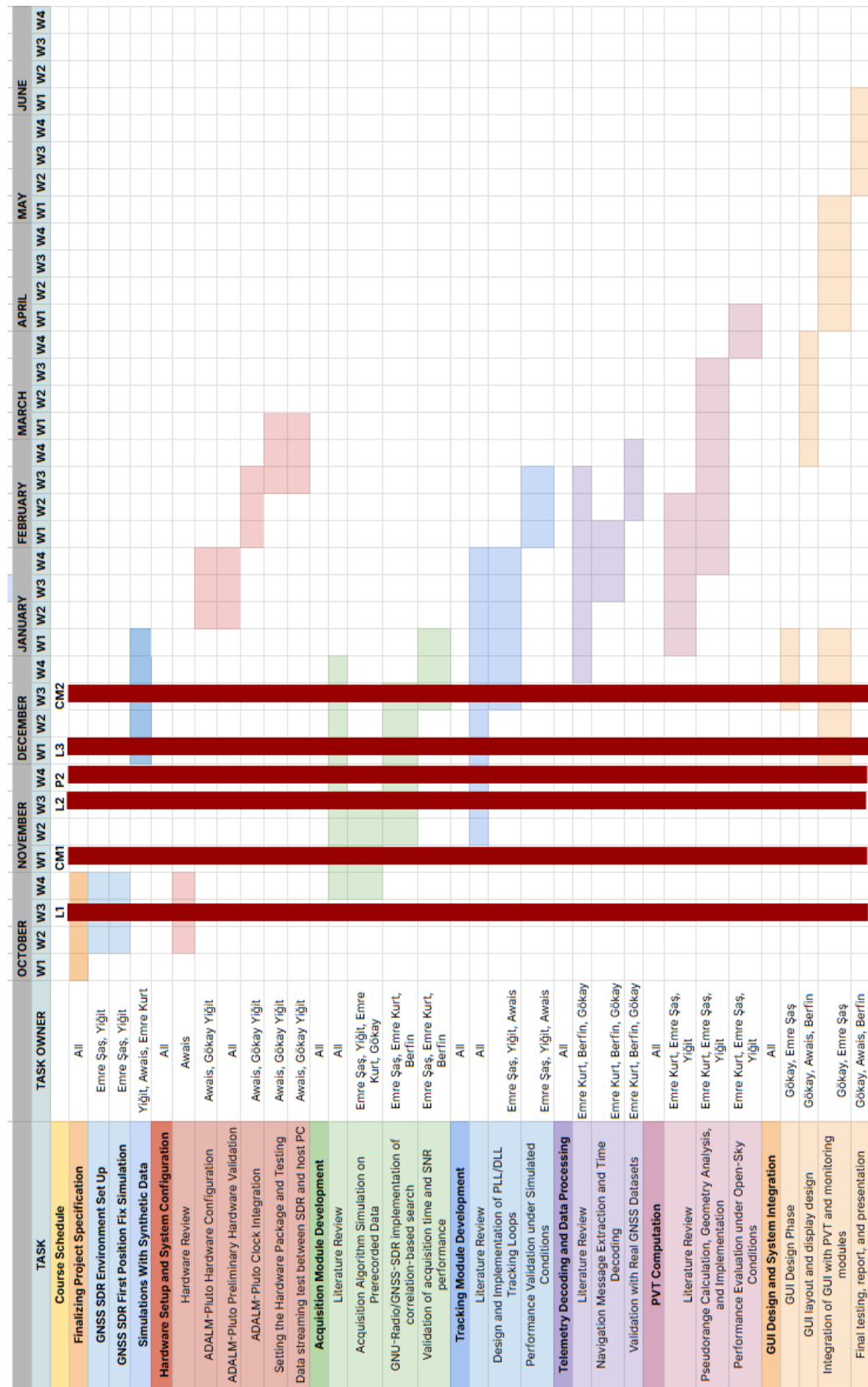


Figure 4: Project Timeline

Appendix D - Changes on Project Timeline since CM1

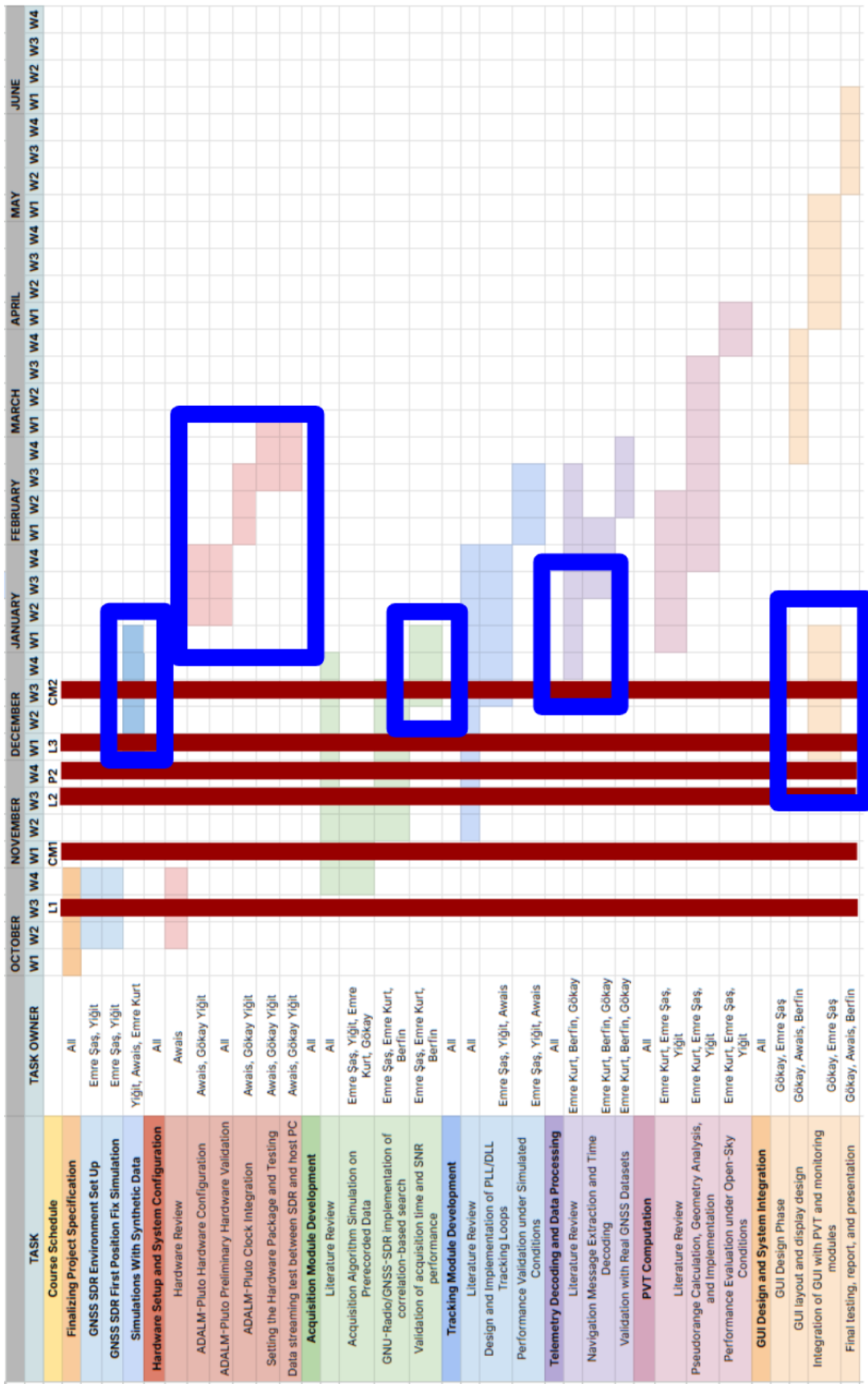


Figure 5: Changes on Project Timeline since CM1.

Appendix E - Specifications of Hardware Pack

Table 5: Technical Specifications of u-blox ANN-MB2-00

Parameter	GPS L1 Band	L5/L2/B3/E6 Band	In context of our project
Frequency range	1535–1602 MHz	1166–1285 MHz	Covers required GPS L1 & L2 bands.
Patch gain	≈ +5 dBic	≈ +4.5 dBic	Directional gain toward sky; reduces ground noise.
LNA gain	31 ± 3 dB	31.5 ± 3 dB	Amplifies the microvolt-level signals to millivolt range.
Noise figure	3 dB	2.5 dB	Adds minimal noise, crucial for weak GNSS signals.
Output VSWR	≈ 2:1	≈ 2:1	Good impedance match to 50 Ω coax.
Cable insertion loss	6.5 dB	5.5 dB	Loss of 5 m RG-174 cable compensated by LNA gain.
Total system gain	≈ 23 dB	≈ 23 dB	What arrives at SDR input.

Table 6: Technical Specifications of Mini-Circuits ZFBT-4R2G+

Parameter	Description
DC Injection	Supplies 3–5 V to the antenna along the coaxial line
RF Passband	10 MHz–4.2 GHz, covering all GNSS bands
Isolation	~40 dB isolation between DC path and RF path which prevents unwanted coupling between the supply and the signal.
Low Loss	<0.7 dB insertion loss at L1/L2

Table 7: Technical Specifications of ADALM-Pluto SDR and Epson TG2520SMN

Parameter	Specification	Relevance to GNSS Receiver
Frequency Range	325 MHz – 3.8 GHz	Covers GPS L1 (1575.42 MHz) & L2 (1227.60 MHz)
ADC Resolution	12-bit I/Q	Adequate for weak GNSS signal dynamic range
Maximum Sample Rate	61.44 MSPS (Effective 4–5 MSPS via USB 2.0)	Meets real-time streaming requirement (HW-FR-1)
RF Gain Control	–10 dB to +70 dB	Full software control
Default Clock Source	Internal 40 MHz XO (± 25 ppm)	Insufficient stability for GNSS tracking
Upgraded Clock Source	Epson TG2520SMN TCXO (40 MHz)	Provides ± 0.5 ppm precision
TXCO Stability	± 0.5 ppm (-40°C to $+85^{\circ}\text{C}$)	Meets HW-FR-2 requirement
TCXO Phase Noise	–161 dBc/Hz @ 100 kHz offset	Enables long coherent integrations
TCXO Power Consumption	~2 mA @ 3.3 V	Suitable for continuous operation

Appendix F - Streamed Parameters for PVT Block

Table 14: Complete list of streamed parameters from PVT Block

Name	Type	Description
tow_at_current_symbol_ms	uint32_t	Time of week of the current symbol, in milliseconds (ms).
week	uint32_t	GPS week number associated with the PVT solution.
rx_time	double	Receiver GPS time.
user_clk_offset	double	User clock offset, in seconds (s).
user_clk_drift_ppm	double	User clock drift, in parts per million (ppm).
utc_time	string	PVT UTC time (RFC 3339 datetime string).
pos_x	double	Position X component in ECEF frame, expressed in meters (m).
pos_y	double	Position Y component in ECEF frame, expressed in meters (m).
pos_z	double	Position Z component in ECEF frame, expressed in meters (m).
vel_x	double	Velocity X component in ECEF frame, expressed in (m/s).
vel_y	double	Velocity Y component in ECEF frame, expressed in (m/s).
vel_z	double	Velocity Z component in ECEF frame, expressed in (m/s).
vel_e	double	East component of velocity in local ENU frame (m/s). (v0.0.19+)
vel_n	double	North component of velocity in local ENU frame (m/s).
vel_u	double	Up component of velocity in local ENU frame (m/s).
cog	double	Course Over Ground, in degrees.
cov_xx	double	Position variance in the X component, σ_x^2 , in m ² .
cov_yy	double	Position variance in the Y component, σ_y^2 , in m ² .

Name	Type	Description
cov_zz	double	Position variance in the Z component, σ_z^2 , in m ² .
cov_xy	double	Position covariance σ_{xy}^2 , in m ² .
cov_yz	double	Position covariance σ_{yz}^2 , in m ² .
cov_zx	double	Position covariance σ_{zx}^2 , in m ² .
latitude	double	Geodetic latitude, in degrees. Positive toward North.
longitude	double	Geodetic longitude, in degrees. Positive toward East.
height	double	Height above reference ellipsoid, in meters (m).
valid_sats	uint32_t	Number of valid satellites used in the solution.
solution_status	uint32_t	RTKLIB solution status indicator.
solution_type	uint32_t	RTKLIB solution type (e.g., 0: xyz-ecef, 1: enu-baseline).
ar_ratio_factor	float	Ambiguity resolution ratio factor used for validation.
ar_ratio_threshold	float	Ambiguity resolution ratio threshold for validation.
gdop	double	Geometric Dilution of Precision (GDOP).
pdop	double	Position (3D) Dilution of Precision (PDOP).
hdop	double	Horizontal Dilution of Precision (HDOP).
vdop	double	Vertical Dilution of Precision (VDOP).

Appendix G - GUI Subsections and Results of Simulation

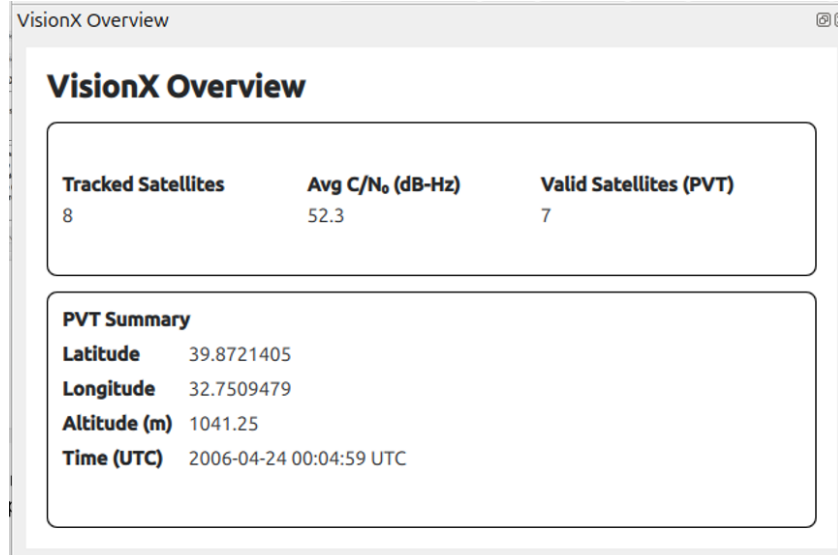


Figure 24: VisionX overview panel displaying receiver status and PVT summary.

The panel shows the number of tracked satellites, average carrier-to-noise density ratio (C/N_0), valid satellites used in the PVT solution, and the decoded latitude, longitude, altitude, and UTC time.

CH	Signal	PRN	ACQ Doppler [Hz]	ACQ Code Phase [samples]	Constellation	C/N ₀ [dB-Hz]	Doppler [Hz]	TOW [ms]	TLM	Pseudorange [m]
0	GPS L1 C/A	1	2500	1170	⊕	55.5	2528.5	86699480	●	2.1874e+07
1	GPS L1 C/A	2	1000	1697	⊖	58.1	882.3	86699500	●	2.08279e+07
2	GPS L1 C/A	3	2750	2285	⊕	51.4	2673.3	86699480	●	2.31937e+07
3	GPS L1 C/A	4	-3750	2494	⊖	51.6	-3656.0	86699480	●	2.38791e+07
4	GPS L1 C/A	5	2750	703	⊕	51.5	2532.6	86699480	●	2.3618e+07
5	GPS L1 C/A	10	-2500	1715	⊖	51.9	-2424.1	86699480	●	2.34647e+07
6	GPS L1 C/A	27	-3750	1160	⊖	49.7	-3657.0	86699480	●	2.38936e+07
7	GPS L1 C/A	9	3250	1878	⊕	48.8	3293.3	86699480	●	2.48318e+07

Figure 25: Per-channel monitoring table obtained from the GNSS-SDR Monitor stream.

The table presents signal- and tracking-level parameters indexed by channel number and PRN, including acquisition Doppler, code phase, real-time Doppler estimates, C/N_0 , time of week (TOW), and pseudorange measurements.

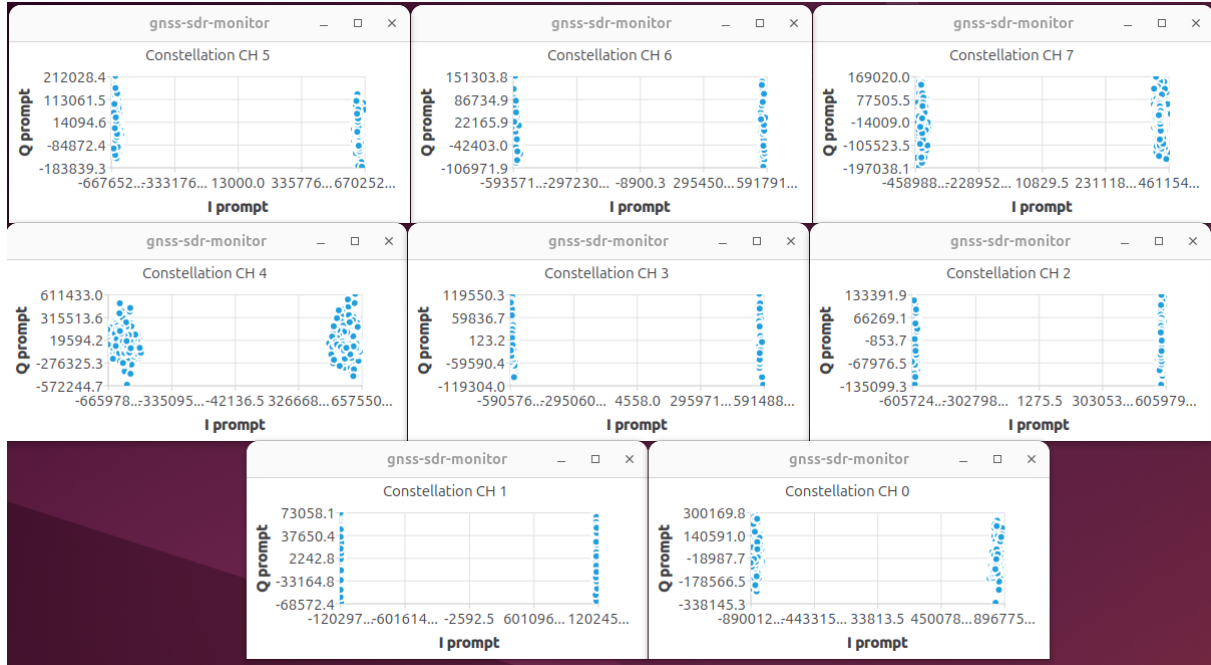


Figure 26: I/Q constellation diagrams for selected tracking channels.

Prompt in-phase (I) and quadrature (Q) correlator outputs are shown for multiple channels, illustrating constellation clustering under stable carrier and code lock conditions.

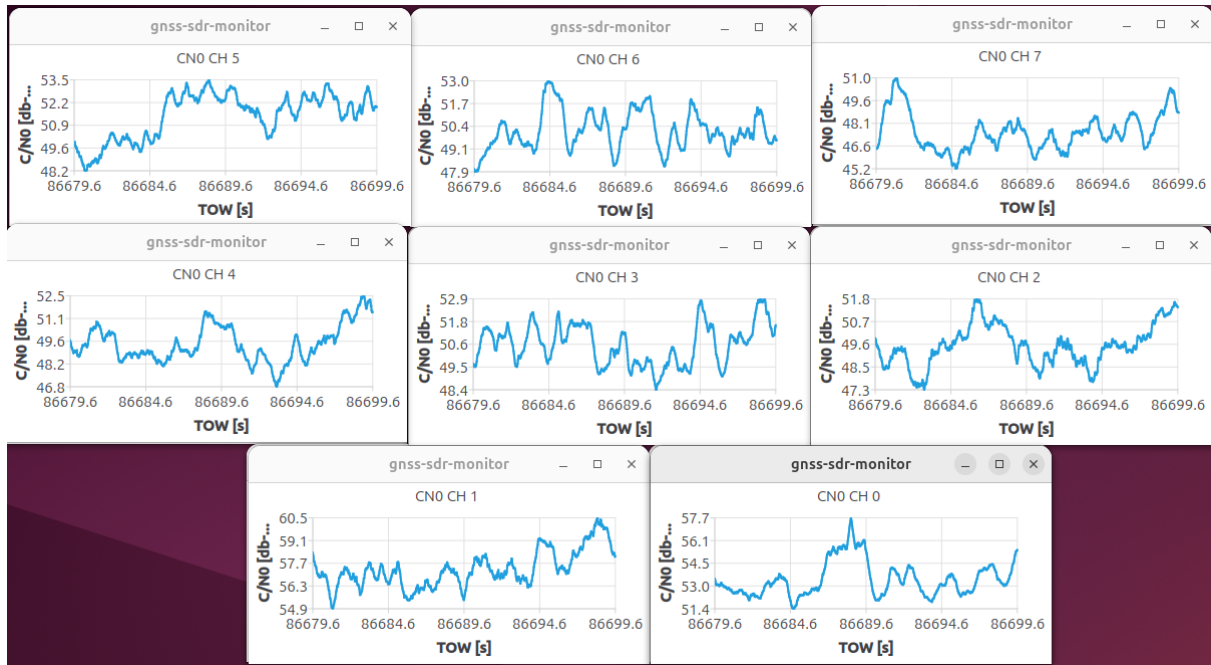


Figure 27: Carrier-to-noise density ratio (C/N_0) versus time for multiple channels.

The plots show the temporal evolution of C/N_0 referenced to GNSS Time of Week (TOW), illustrating signal strength stability during the synthetic dataset simulation.

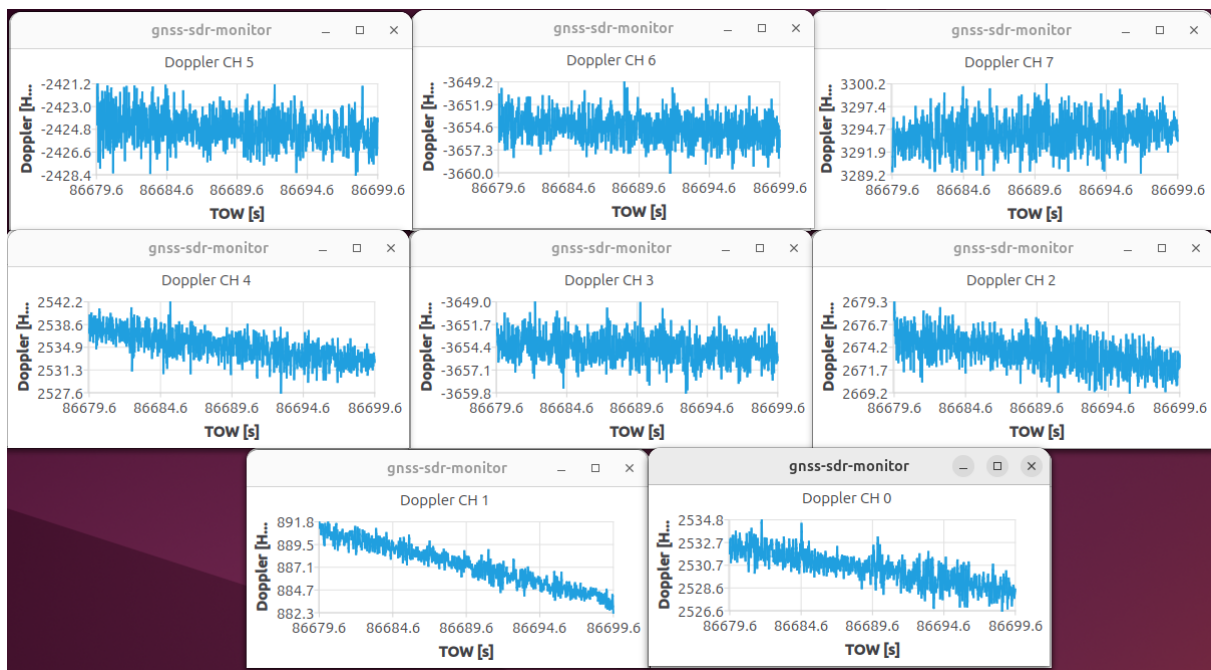


Figure 28: Doppler frequency estimates versus time for multiple channels.

Carrier Doppler estimates are shown as a function of TOW, reflecting stable frequency tracking behavior across all active channels.



Figure 29: Map-based visualization of estimated receiver positions.

Estimated positions from the PVT solution are displayed on a map interface, showing spatial clustering around a fixed location during the synthetic static scenario.

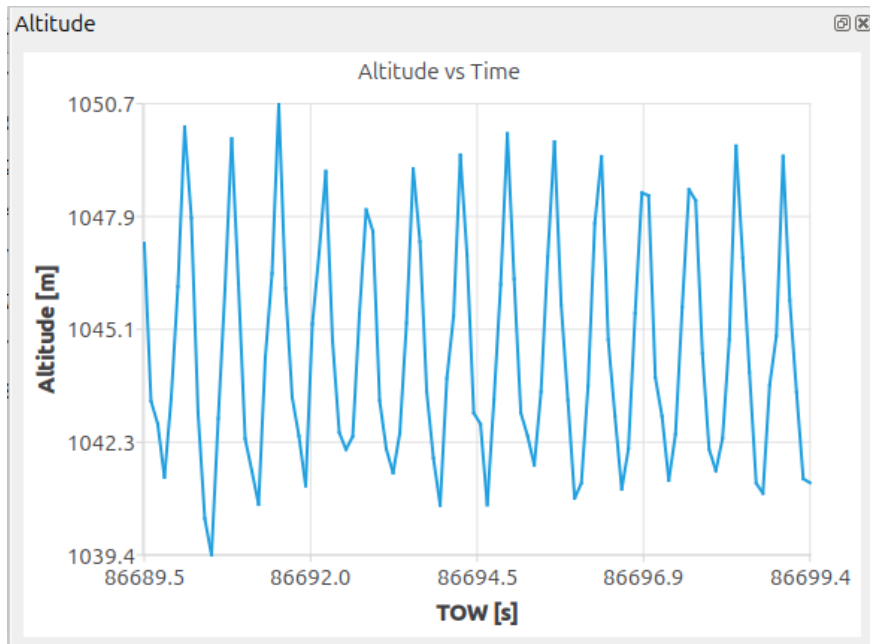


Figure 30: Altitude estimates versus time.

The altitude component of the PVT solution is plotted as a function of TOW, illustrating bounded vertical fluctuations typical of GNSS positioning.

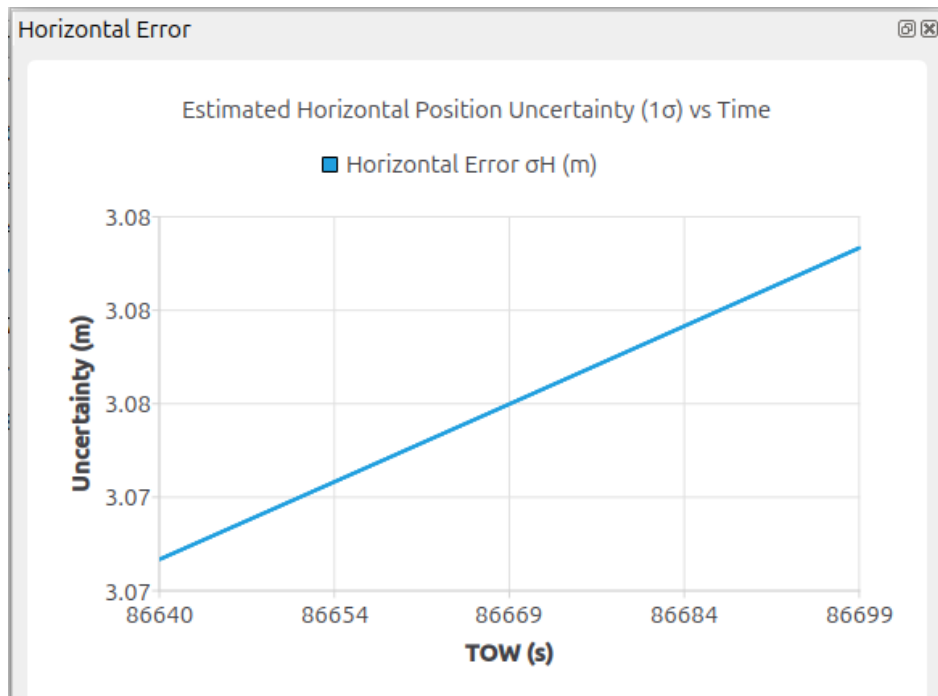


Figure 31: Estimated horizontal position uncertainty (1σ) versus time.

The plot shows the covariance-derived horizontal uncertainty reported by the navigation filter, expressed as a function of GNSS Time of Week.

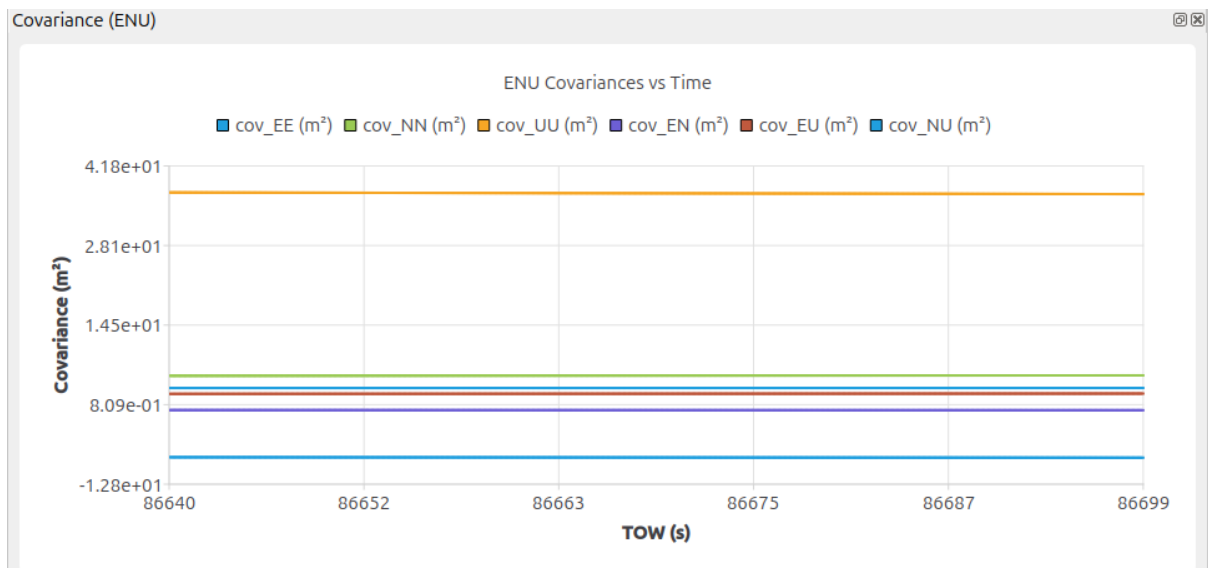


Figure 32: ENU covariance matrix components versus time.

Diagonal and off-diagonal elements of the position covariance matrix in the local ENU frame are shown, illustrating estimator uncertainty structure over time.



Figure 33: ENU velocity components versus time.

East, North, and Up velocity components are plotted as a function of TOW, showing near-zero mean behavior consistent with a static synthetic receiver scenario.

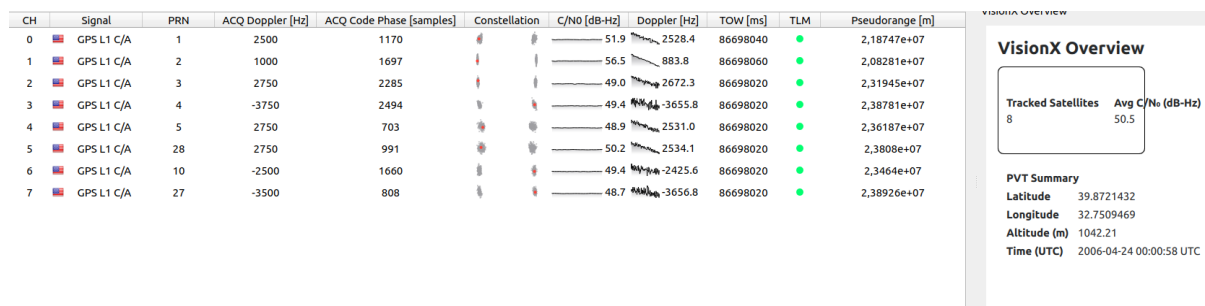


Figure 34: Noisy Synthetic Data GNSS SDR Results. The carrier to noise ratio is reduced now to around 50 dB-Hz.

Appendix H - Positional Accuracy Metrics

Table 16: Available Positional Accuracy metrics for GNSS signals

Measure	Formula	Confidence Region Probability	Definition
2DRMS	$2\sqrt{\sigma_E^2 + \sigma_N^2}$	95 %	Twice the DRMS of the horizontal position errors, defining the radius of a circle centered at the true position, containing the horizontal position estimate with a probability of 95 %.
DRMS	$\sqrt{\sigma_E^2 + \sigma_N^2}$	65 %	The square root of the average of the squared horizontal position errors, defining the radius of a circle centered at the true position, containing the horizontal position estimate with a probability of 65 %.
CEP	$0.62\sigma_N + 0.56\sigma_E$ (accurate if $\frac{\sigma_N}{\sigma_E} > 0.3$)	50 %	The radius of a circle centered at the true position, containing the horizontal position estimate with a probability of 50 %.
99 % Spherical Accuracy Standard	$1.122(\sigma_E^2 + \sigma_N^2 + \sigma_U^2)$	99 %	The radius of a sphere centered at the true position, containing the position estimate in 3D with a probability of 99 %.
90 % Spherical Accuracy Standard	$0.833(\sigma_E^2 + \sigma_N^2 + \sigma_U^2)$	90 %	The radius of a sphere centered at the true position, containing the position estimate in 3D with a probability of 90 %.
MRSE	$\sqrt{\sigma_E^2 + \sigma_N^2 + \sigma_U^2}$	61 %	The radius of a sphere centered at the true position, containing the position estimate in 3D with a probability of 61 %.
SEP	$0.51(\sigma_E^2 + \sigma_N^2 + \sigma_U^2)$	50 %	The radius of a sphere centered at the true position, containing the position estimate in 3D with a probability of 50 %.